Title: Global glacier change in the 21st century: Every increase in temperature matters

Authors: David R. Rounce[1,2*], Regine Hock[2,3], Fabien Maussion[4], Romain Hugonnet[5,6,7], William Kochtitzky[8,9], Matthias Huss[5,6,10], Etienne Berthier[7], Douglas Brinkerhoff[11], Loris Compagno[5,6], Luke Copland[8], Daniel Farinotti[5,6], Brian Menounos[12,13], Robert W. McNabb[14]

Affiliations:

[1]Department of Department of Civil & Environmental Engineering, Carnegie Mellon University; Pittsburgh, PA, USA

[2]Geophysical Institute, University of Alaska Fairbanks; Fairbanks, AK, USA

[3]Department of Geosciences, University of Oslo; Oslo, Norway

[4]Department of Atmospheric and Cryospheric Sciences, University of Innsbruck; Innsbruck, Austria

[5]Laboratory of Hydraulics, Hydrology and Glaciology (VAW), ETH Zürich; Zurich, Switzerland

[6]Swiss Federal Institute for Forest, Snow and Landscape Research (WSL); Birmensdorf, Switzerland

[7]LEGOS, Université de Toulouse, CNES, CNRS, IRD, UPS; Toulouse, France

[8]Department of Geography, Environment and Geomatics, University of Ottawa; Ottawa, Ontario, Canada

[9]School of Marine and Environmental Programs, University of New England, Biddeford, Maine, USA

[10]Department of Geosciences, University of Fribourg; Fribourg, Switzerland

[11]Department of Computer Science, University of Montana; Missoula, MT, USA

[12]Geography Earth and Environmental Sciences, University of Northern British Columbia; Prince George, BC, Canada

[13]Hakai Institute; Campbell River, BC, Canada

[14]School of Geography and Environmental Sciences, Ulster University; Coleraine, UK

*Corresponding author. Email: drounce@cmu.edu

Abstract: Glacier mass loss impacts sea-level rise, water resources, and hazards. We present global glacier projections, excluding the ice sheets, for Shared Socioeconomic Pathways calibrated with data for each glacier. Glaciers are projected to lose 26±6% (+1.5°C) to 41±11% (+4°C) of their mass by 2100, relative to 2015, for global temperature change scenarios. This corresponds to 90±26 to 154±44 mm sea level equivalent and causes 49±9% to 83±7% of glaciers to disappear. Mass loss is linearly related to temperature increase, thus reductions in temperature increase reduce mass loss. Based on climate pledges from the Conference of Parties

(COP-26) global mean temperature is projected to increase by +2.7°C, which would lead to a sea-level contribution of 115±40 mm and cause widespread deglaciation in most mid-latitude regions.

One-Sentence Summary: Projected glacier mass loss stresses urgency of limiting global warming to reduce sea-level rise and widespread deglaciation.

Main Text: Glaciers, here referring to all glacial land ice excluding the Greenland and Antarctic ice sheets, are responsible for 21±3% of sea-level rise from 2000-2019, contributing 0.74±0.04 mm sea level equivalent (SLE) yr^{-1} (*1*). Projections suggest this contribution could increase to 2.5 mm SLE yr^{-1} by 2100 (*2*). Glaciers are also a critical water resource for ~1.9 billion people (*3*), and projected losses will alter water availability impacting annual and seasonal runoff (*4*). Glacier-related hazards, including glacier outburst floods, are also expected to change in frequency and magnitude over the next century due to mass loss (*5*). Projecting the magnitude, spatial pattern and timing of glacier mass loss is therefore essential to support climate adaptation and mitigation efforts for communities ranging from the coast to the high mountains.

Previous projections of glacier mass loss from the Glacier Model Intercomparison Project (GlacierMIP) (2) estimated glacier contribution to sea-level rise for ensembles of Representative Concentration Pathways (RCPs), and results were extended to Shared Socioeconomic Pathways (SSPs) using statistical models of these simulations (*6*). GlacierMIP provided these projections at regional scales based on simulations from 11 glacier evolution models that varied with respect to the complexity of model physics, simulated physical processes, model calibration, spatial resolution, and modeling domain. Calibration data varied from in-situ measurements of less than 300 of the world's more than 215,000 glaciers to regional geodetic and/or gravimetric mass balance observations. Furthermore, only one global model simulated glacier dynamics using a flowline model (*7*), while all others relied on empirical volume-area scaling or parameterizations of mass redistribution; only one model accounted for frontal ablation (i.e., the sum of iceberg calving and submarine melt) of marine-terminating glaciers (*8*), while all others treated any glacier as land-terminating; and no global model accounted for debris cover. Existing multi-model projections (*2*, *6*, *9*) are thus limited to regional scales and neglect key physical processes controlling glacier mass loss.

Here we produce a set of global glacier projections for every individual glacier on Earth for SSPs from 2015 to 2100 by leveraging global glacier mass balance data (*1*) and nearly-global frontal ablation data (*10–13*). To provide policy-relevant scenarios, our projections are grouped based on mean global temperature increases by the end of the 21st century compared to pre-industrial levels to explicitly link differences in glacier mass loss, sea-level rise, and the number of glaciers that vanish in response to changes in mean global temperature. Our glacier evolution model, a hybrid of the Python Glacier Evolution Model (PyGEM) (*14*, *15*) and Open Global Glacier Model (OGGM) (*7*), enables us to produce global glacier projections that explicitly account for glacier dynamics using a flowline model (*7*) based on the shallow-ice approximation (*16*); the effects of debris thickness on sub-debris melt rates (*17*), and frontal ablation (*8*). Our estimates of glacier contribution to sea-level rise also account for the roughly 15% of ice from marine-terminating glaciers that is already below sea level (*18*). Projections are also reported for SSPs and RCPs to highlight differences compared to previous studies.

Projections of policy-relevant scenarios

The Paris Agreement, adopted in 2015 by 195 countries, agreed to keep the increase in global mean temperature by the end of the 21st century relative to pre-industrial levels below 2°C, and that efforts should be made to limit the temperature change to 1.5°C. This target was kept alive in the Glasgow Agreement adopted by the Conference of the Parties (COP26) in 2021. To evaluate the sensitivity of glaciers to global mean temperature increases, the glacier projections are aggregated into +1.5°C, +2°C, +3°C, and +4°C temperature change scenarios by 2100 relative to pre-industrial levels (Fig. 1).

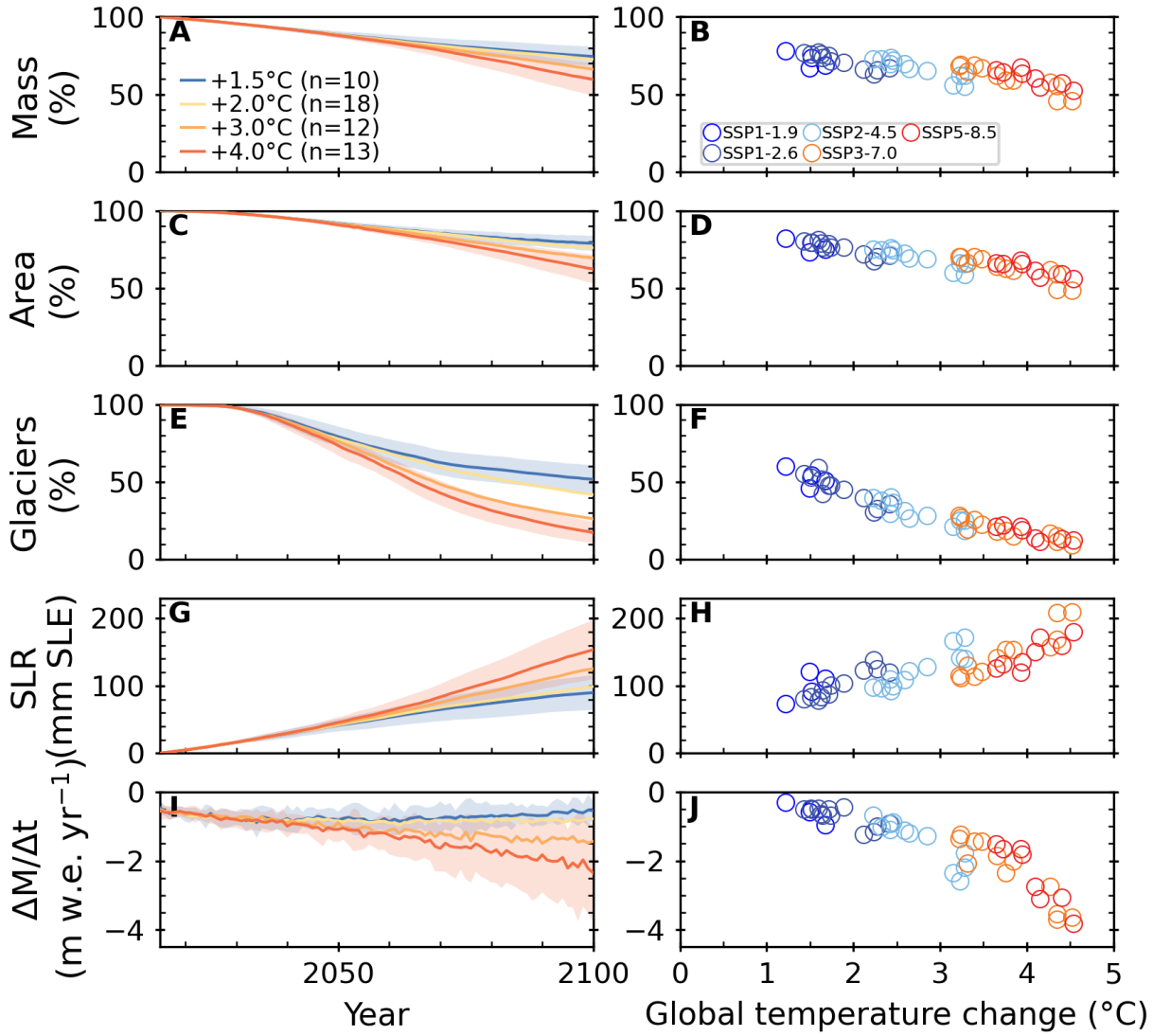

Fig. 1. Projected global glacier changes for scenarios of global mean temperature change. (A, B) Mass remaining, (C, D) area remaining, (E, F) glaciers remaining, (G, H) sea-level rise (SLR) contributed from glaciers, and (I, J) area-averaged mass change rate for all glaciers globally. Projections are shown from 2015 to 2100 (left panels), and at 2100 (right panels). Values in (A) - (H) are relative to 2015. Colors depict the global mean temperature change scenarios (left panels) and the SSPs corresponding to the global temperature changes (right panels). The number (n) of glacier projections with different GCMs and SSPs that fall into each temperature change scenario is shown in the legend. Lines (left panels) show the ensemble median and shading indicates the 95% confidence interval for each temperature change scenario.

Globally, glaciers are projected to lose 26±6% (+1.5°C) to 41±11% (+4°C) of their mass by 2100, relative to 2015 (ensemble median ± 95% confidence interval). This mass loss would increase mean sea level by 90±26 mm SLE under the +1.5°C scenario and 99±31 mm SLE under the +2°C scenario. The higher temperature change scenarios of +3°C and +4°C lead to

contributions of 125±39 and 154±44 mm SLE, respectively, highlighting a 71% increase between the +1.5°C and +4°C scenarios.

The rate of sea-level rise from glacier losses near the end of the 21st century ranges from 0.70±0.45 to 2.23±1.08 mm SLE yr^{-1} depending on the temperature change scenario (Fig. S1). For +1.5°C, the rate of sea-level rise peaks at 1.29±0.59 mm SLE yr^{-1} around 2035 and declines thereafter, while the rate for +4°C steadily increases for the remainder of this century. Similar trends are observed in the area-averaged mass loss rate, where the maximum loss rate of 0.82±0.36 m water equivalent (w.e.) yr^{-1} occurs around 2035 before diminishing to 0.59±0.34 m w.e. yr^{-1} at the end of the century for the +1.5°C scenario; the mass loss rate continuously increases to 2.02±1.30 m w.e. yr^{-1} by the end of the century for the +4°C scenario (Fig. 1I). Even if the global mean temperature change is limited to +1.5°C, we estimate that 104,000±20,000 glaciers (49±9% of the total inventoried) will disappear by 2100 and at least half of those will be lost prior to 2050 (Fig. 1E). Most of the glaciers projected to disappear are smaller than 1 km^2 (Fig. 2), but despite their small size their disappearance may still negatively impact local hydrology, tourism, glacier hazards, and cultural values (*19*). Glaciers projected to disappear represent 2-8% of the glacier contribution to sea-level rise depending on the temperature change scenario.

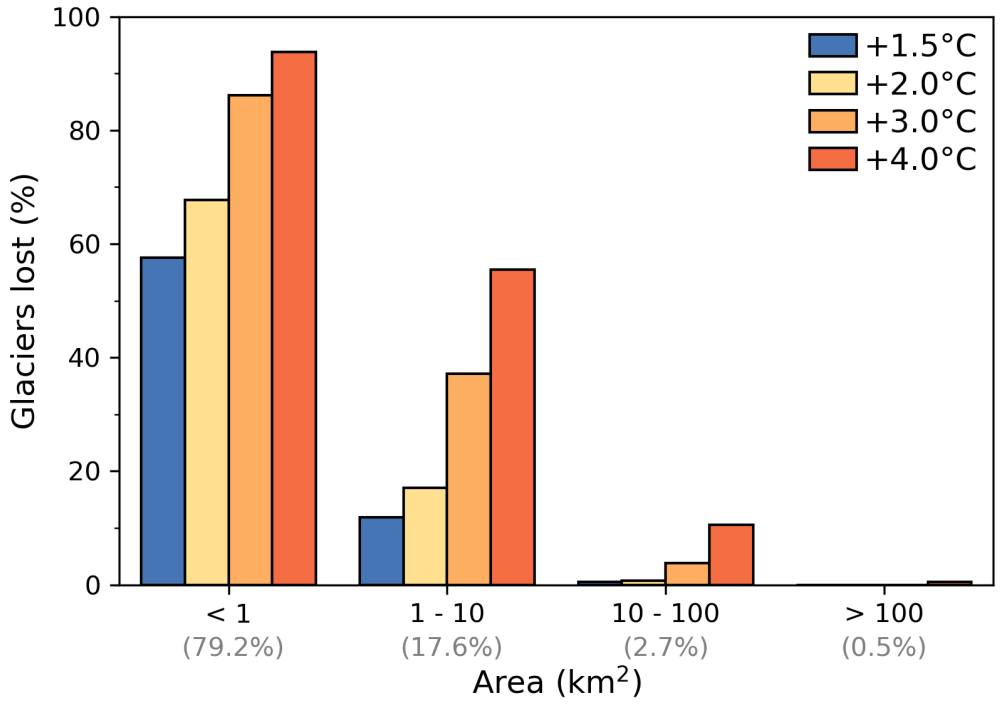

Fig. 2. Percent of glaciers projected to vanish between 2015 and 2100 for global temperature change scenarios sorted by size. The glaciers are binned according to their initial glacier area and the numbers below each bin (shown in grey) refer to the percentage of the total number of glaciers in 2015 in each bin.

Regional mass changes

Regional variations exist in the glacier mass change projections (Fig. 3). Alaska is the largest regional contributor to global mean sea-level rise from 2015 to 2100 (Fig. S2), peaking at 0.33 to 0.44 mm SLE yr^{-1} between 2030 and 2060 depending on the temperature change scenario, before

decreasing to 0.13 to 0.28 mm SLE yr^{-1} by 2100 (Fig. S1). Greenland Periphery, Antarctic and Subantarctic, Arctic Canada North, and Arctic Canada South contribute 12, 10, 10, and 9% to projected sea-level rise, respectively. Collectively, these five regions account for 60-65% of the total glacier contribution to sea-level rise. For Greenland Periphery, Arctic Canada North, and Arctic Canada South, the rate of the contribution to sea-level rise is almost insensitive to temperature change below +2°C, but steadily increases through 2100 for the other temperature change scenarios. For the +3°C and +4°C scenarios, the rate of sea-level rise from Greenland Periphery, Antarctic and Subantarctic, and Arctic Canada North each nearly equal or exceed Alaska near the end of the century, with Antarctic and Subantarctic and Arctic Canada North accelerating throughout the 21st century. Since projected glacier mass loss includes both the instantaneous response of glaciers to climate forcing and the delayed response based on the extent of disequilibrium to longer-term climatic conditions (e.g., *20*), these regions with large glaciers will continue losing mass beyond 2100, especially for higher temperature change scenarios.

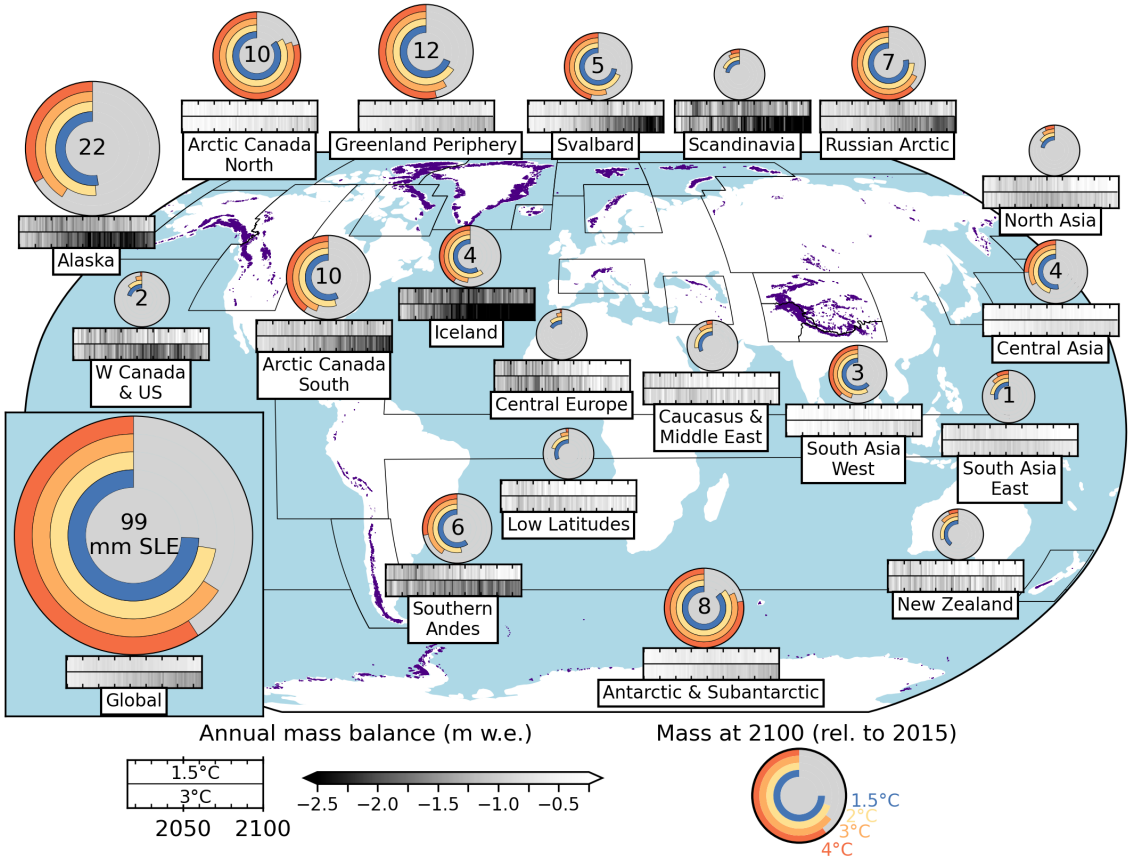

Fig. 3. Regional glacier mass change and contributions to sea level rise from 2015 to 2100. Discs show global and regional projections of glacier mass remaining by 2100, relative to 2015, for global mean temperature change scenarios. Discs are scaled based on each region's contribution to global mean sea level rise from 2015 to 2100 for the +2°C scenario by 2100 relative to pre-industrial levels and nested rings are colored by temperature change scenarios showing normalized mass remaining in 2100. Regional sea level rise contributions larger than 1 mm SLE for the +2°C scenario are printed in the center of the pie chart. The horizontal bars show time series of area-averaged annual mass balance from 2015 to 2100 for +1.5°C (top) and

+3°C (bottom) scenarios. The colorbar is saturated at -2.5 m w.e., but minimum annual values reach -4.2 m w.e. in Scandinavia. Time series of regional relative mass change and regional area-averaged mass change are shown in Figs. S3-4.

Western Canada and US, South Asia East, Scandinavia, North Asia, Central Europe, Low Latitudes, Caucasus and Middle East, and New Zealand, are projected to lose 60-100% of their glacier mass depending on the temperature change scenario (Figs. 3, S3). The temperature change scenario thus has a major impact on the mass loss, in some cases determining whether the complete deglaciation of regions occurs by the end of the 21st century. While these regions are not significant contributors to sea-level rise, people in these regions will need to adapt to changes in seasonal and annual runoff as the additional water provided by glacier net mass loss will decline before 2050 as the glaciers retreat (Figs. S5-8). In High Mountain Asia, the timing of maximum rates of mass loss varies, with South Asia East peaking between 2025-2030, Central Asia between 2035-2055, and South Asia West between 2050-2075, depending on the temperature change scenario.

Regional sensitivity to temperature change

The sensitivity of the glacierized regions to changes in global mean temperature depends on the region's current glacier mass and mass change rates; regional temperature anomalies relative to the global mean (Fig. 4), such as those associated with Arctic amplification (*21*); the climatic setting (maritime versus continental) and sensitivity to precipitation falling as rain instead of snow; and elevation feedbacks due to different types of glaciers (e.g., ice caps versus valley glaciers) (*22*). Projected mass loss is linearly related to global mean temperature increase, especially for larger glacierized regions, consistent with a recent study (*6*). This strong relationship highlights that every fraction of a degree of temperature increase significantly impacts glacier mass loss. The smallest glacierized regions by mass, including Central Europe, Scandinavia, Caucasus and Middle East, North Asia, Western Canada and US, Low Latitudes, and New Zealand, will experience near-complete deglaciation around +3°C. These regions are thus highly sensitive to global mean temperature increases between 1.5 and 3°C and have a nonlinear response above 3°C of warming.

The strength of the linear relationship varies among regions, which reflects differences in the regional temperature anomalies from the ensemble of GCMs (evident from the larger standard deviations given in Figs. 4, S9). Regions like Alaska, Southern Andes, and Central Asia have less scatter indicating less variation in the regional temperature anomaly and thereby a more consistent response to climate forcing (mean R^2=0.78). Other regions like the Russian Arctic, Svalbard, and Iceland have more variation in the regional temperature anomaly and thus a weaker linear relationship (mean R^2=0.50) as well as significant variations in projected precipitation (Fig. S10). Future work using regional climate projections may better resolve high-mountain climatic conditions and refine projections in these regions (e.g., *22*).

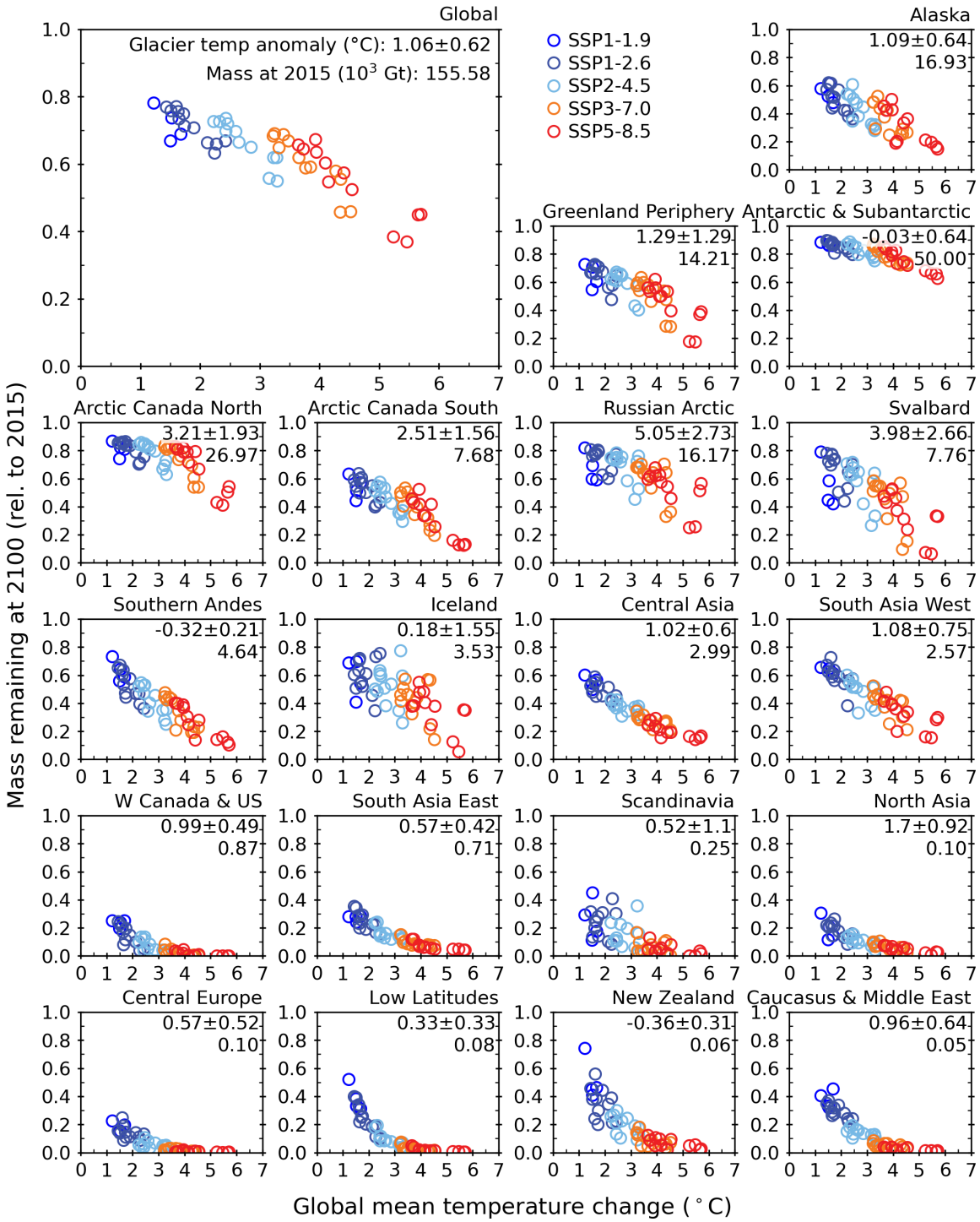

Fig. 4. Fraction of global and regional mass remaining at 2100, relative to 2015, as a function of global mean temperature change by 2100 relative to pre-industrial levels. Each marker represents results from one GCM and SSP. Numbers indicate median temperature anomalies (± standard deviation) (°C) over glacierized areas, relative to the mean temperature change over the entire globe at 2100 relative to pre-industrial levels, for all GCMs and scenarios, and the glacier mass at 2015 (10^3 Gt). Negative values indicate that some regions warm less than the global average. Regions are ordered by their total mass loss.

Spatially resolved projections at glacier scale

Our projections reveal notable spatial variations in glacier mass loss at the local scale for the temperature change scenarios (Fig. 5). All regions are projected to lose some glaciers completely, primarily smaller ice masses, with the higher temperature change scenarios revealing significantly more mass loss and the deglaciation of greater areas (Figs. S11-13). While Central Europe, Caucasus and Middle East, North Asia, and Western Canada and US are projected to experience widespread deglaciation for the +2°C scenario, our results also reveal where remaining glaciers will be concentrated at the end of this century. Besides the Karakoram and Kunlun in High Mountain Asia, the remaining mass is primarily located in southeastern Alaska, Arctic Canada North, Svalbard, the Russian Arctic, Greenland Periphery, and Antarctic and Subantarctic. Given that these regions comprise a significant number of marine-terminating glaciers, accounting for frontal ablation is critical over the next century and beyond.

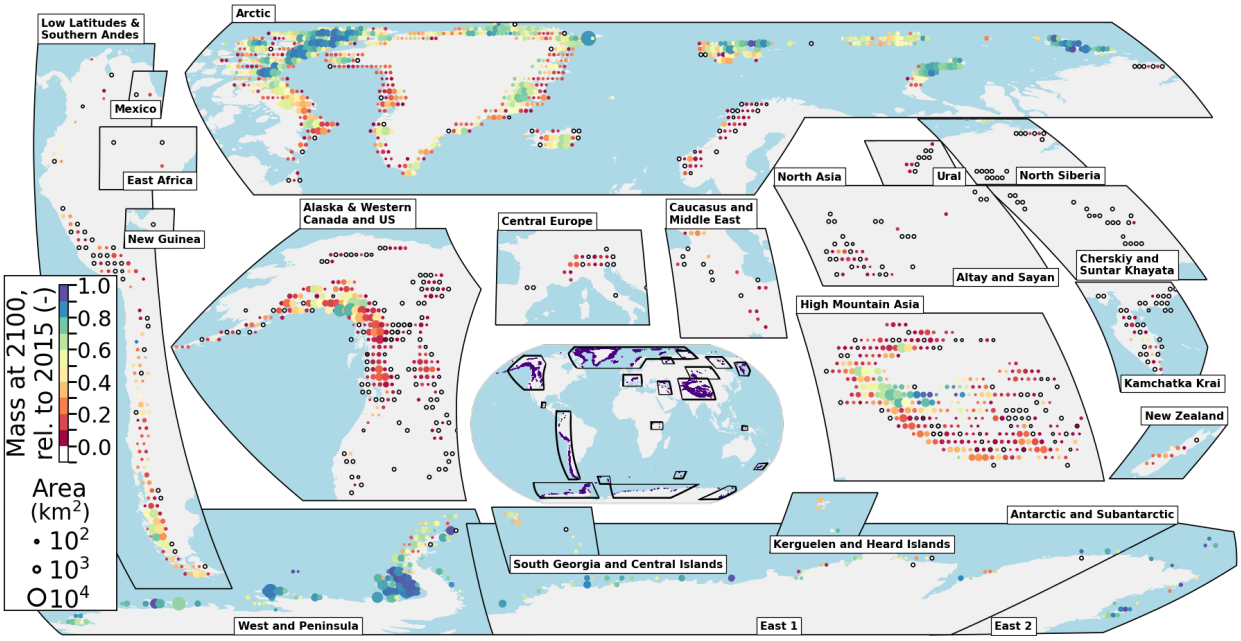

Fig. 5. Spatial distribution of glacier mass remaining by 2100 for the +2°C scenario. The ensemble median glacier mass remaining by 2100 (relative to 2015) for the +2°C (above pre-industrial levels) global mean temperature change scenario. Tiles are aggregated by 1°x1° below 60° latitude, 2°x1° between 60° and 74° latitude and 2°x2° above 74° latitude to represent approximately 10,000 km^2 each. Circles are scaled based on simulated glacierized area in 2015 and are colored by normalized mass remaining. Regions that have experienced complete deglaciation by 2100 are shown in white and outlined in black. High Mountain Asia refers to Central Asia, South Asia West, and South Asia East. Specific subregions are noted by labels on the bottom of inset figures. Additional temperature change scenarios (+1.5, +3, and +4 °C) are shown in Figs. S11-13.

Importance of marine-terminating glaciers

Marine-terminating glaciers represent 40% of the total present-day global glacier area (*23*), and this percentage reaches 99% for the Antarctic and Subantarctic region. Most previous global glacier projections do not explicitly account for frontal ablation (*2*), instead implicitly accounting for it by increasing melt rates, thereby poorly accounting for dynamical feedbacks associated

with the glacier's evolution. Our model couples a frontal ablation parameterization with a flowline model and uses a state-of-the-art calibration scheme, ice thickness inversion method, and geodetic mass balance and frontal ablation calibration data (see Methods). This enables us to project changes of individual marine-terminating glaciers and determine if and when they become land-terminating (Fig. S14). Separate simulations including and excluding frontal ablation, with model parameters calibrated separately for both, are used to quantify its impact on projections.

Counterintuitively, we estimate that accounting for frontal ablation reduces the glacier contribution to mean sea-level rise from 2015-2100 by 2% for each temperature change scenario, compared to models not including frontal ablation. From 2015-2100 frontal ablation accounts for 91±10 Gt yr^{-1} (+1.5°C) to 88±8 Gt yr^{-1} (+4°C) of the total glacier mass loss globally (Figs. S15-18). For the +2°C scenario, the rate of mass loss due to frontal ablation diminishes over the century from 115±11 Gt yr^{-1} in 2000-2020 to 75±8 Gt yr^{-1} in 2080-2100. Diminished mass losses from frontal ablation of marine-terminating glaciers reflect their thinning, retreat onto land (44-57% of all marine-terminating glaciers) (Fig. S19), and reduced ice flux into the ocean, which occurs for all temperature change scenarios. The relative contribution of frontal ablation to total ablation (i.e., frontal ablation plus melt) ranges from 11% (+1.5°C) to 8% (+4°C) for 2015-2100, diminishing for higher temperature change scenarios due to increases in melt. Regionally, the relative contribution of frontal ablation for all temperature change scenarios is greatest in Antarctic and Subantarctic (34%), the Russian Arctic (34%), and Svalbard (17%) (Figs. S15-18).

The impact of not accounting for frontal ablation on relative mass loss (i.e., glacier mass loss by 2100 relative to 2015) varies greatly by region (Fig. S20). For Alaska and Svalbard, excluding frontal ablation increases relative mass loss at 2100 by 2-8% depending on the temperature change scenario. The Russian Arctic varies from a 2% reduction (+1.5°C) to a 5% increase (+4°C). Arctic Canada, Greenland Periphery, and Southern Andes see almost no difference (±2%), and Antarctic/Subantarctic sees a 0-2% decrease in relative mass loss. These results highlight the complex response of marine-terminating glaciers, which are dependent on the frontal ablation rate, glacier geometry, and surface mass balance. In the Antarctic and Subantarctic, we find excluding frontal ablation decreases the regional relative mass loss, since mass loss due to frontal ablation is greater than the increased melt when frontal ablation is excluded. Conversely, in Alaska and Svalbard, the regional relative mass loss increases when frontal ablation is excluded, since mass loss due to frontal ablation is less than the increased melt when frontal ablation is excluded.

Importance of debris-covered glaciers

Debris currently covers 4-7% of the global glacier area (*24*, *25*). A thin layer of debris (< 3-5 cm) enhances surface melt, while a thick layer insulates the underlying ice and reduces melt (*26*). The spatial distribution of debris thickness can cause debris-covered glaciers to develop stagnant glacier tongues and eventually separate from the active part of the glacier (*27*, *28*). Our representation of debris and glacier dynamics enables us to simulate these complex feedbacks, including reduced melt at glacier termini where debris is thick (Fig. S21). We thus produce a set of global glacier projections that account for debris and compare these to separate simulations that exclude debris (i.e., treat the debris as clean ice) to quantify the insulating effect that debris has on glacier projections.

The impact of debris on relative mass loss varies greatly spatially and temporally (Fig. S22) with the most significant differences occurring in the mid-century in New Zealand and South Asia

East. In these regions, the insulating effect of debris reduces net mass loss by 9-13% depending on the temperature change scenario, although the differences are less than 5% by 2100. Alaska, the largest region by mass with considerable debris cover (>5% by area), sees a reduction of 5% around 2060 and 3% by 2100. Other regions with considerable debris cover (> 5% by area), including Western Canada and US, Central Europe, Caucasus and Middle East, and Low Latitudes, see a reduction in mass loss of less than 5% in the mid-century and no difference (±1%) by 2100. The inclusion of debris thus delays mass loss over the century, especially at local scales, but has little impact on sea-level rise and the number of glaciers lost by 2100. The limited impact in most regions shows that the insulating effect of debris is unable to offset the increased melt for the various temperature change scenarios.

Comparison with previous projections

For comparison with recent multi-model studies (*2*, *6*), we also report our projections for the RCPs and SSPs. Our global projections of glacier contribution to sea-level rise for 2015-2100 range from 90±36 mm SLE (RCP2.6) to 163±53 mm SLE (RCP8.5) and 98±38 mm SLE (SSP1-2.6) to 166±83 mm SLE (SSP5-8.5), respectively (Table 1). These projections include a correction (reduction) of 17 to 24 mm SLE, which accounts for the mass loss of ice from marine-terminating glaciers that is below sea level and therefore will not contribute to global mean sea-level rise; an important difference compared to the current multi-model studies (*2*, *6*) which do not account for this. Even with this correction, for the low emissions scenarios our RCP2.6 projections are 11 mm SLE (14%) greater than Marzeion et al. (*2*), and our SSP1-2.6 projections are 18 mm SLE (23%) greater than Edwards et al. (*6*). For the mid-range (RCP4.5 and SSP2-4.5) and high (RCP8.5, SSP5-8.5) emissions scenarios, our projections are within ±7 mm SLE of than both studies.

Table 1. Projected global glacier mass loss and glacier contribution to sea-level rise. Results are shown for RCP and SSP scenarios at 2100, relative to 2015, from this study and recent multi-model studies (*2*, *6*). 'Uncorrected' refers to projections that assume mass losses below sea level contribute to sea-level rise, consistent with assumptions in recent multi-model studies. Note that uncertainty associated with the multi-model studies is expressed as 90% confidence interval, while this study reports ensemble median and 95% confidence interval. Regional comparisons are shown in Tables S1-2.

Global glacier contribution to sea-level rise from 2015 to 2100 (mm SLE)						
Study	RCP2.6	RCP4.5	RCP8.5	SSP1-2.6	SSP2-4.5	SSP5-8.5
This study	90±36	114±44	163±53	98±38	116±51	166±83
This study (uncorrected)	106±37	132±47	187±61	115±42	135±57	192±97
Marzeion et al. (*2*)	79±57	119±66	159±86	-	-	-
Edwards et al. (*6*)	-	-	-	80±35	119±39	159±47
Global glacier mass loss, relative to 2015 (%)						
Study	RCP2.6	RCP4.5	RCP8.5	SSP1-2.6	SSP2-4.5	SSP5-8.5
This study	26±8	31±10	43±13	28±9	32±12	44±20
Marzeion et al. (*2*)	18±13	27±15	36±20	-	-	-

Not correcting for the loss of ice below sea level, our projections of glacier contribution to sea-level rise from 2015-2100 are 11-44% greater than these multi-model estimates (*2*, *6*) for all emission scenarios. We attribute these differences to the global mass balance data we used for calibration, which include an accelerated trend in mass loss from 2000-2020 (*1*), as well as the improved representation of physical processes in our model.

Globally, we predict glaciers will lose 26±8% (RCP2.6) to 43±13% (RCP8.5) and 28±9% (SSP1-2.6) to 44±20% (SSP5-8.5) of their mass by 2100, relative to 2015. Our projected relative mass losses are 4-8% greater than current multi-model estimates (*2*). Regionally, the most significant differences occur in Alaska, Arctic Canada South, South Asia East, and Southern Andes, where we predict 11-23% more relative mass loss (Table S1). In Alaska, we estimate 22% (RCP2.6) to 23% (RCP8.5) more relative mass loss compared to the multi-model estimates (*2*), and find a peak in the net mass loss rate in the middle of the century, in contrast to the peak net mass loss rate at the end of the century from the multi-model estimates (*2*).

A comparison of our projections from the ensembles of RCPs and SSPs used in this study reveals that glacier contribution to sea-level rise is 2-9% greater for SSPs than the corresponding RCPs. These differences are a result of the SSPs simulating greater temperature increases for the same radiative forcing as the RCPs (*29*, *30*). Our ensembles reflect this higher warming sensitivity as our SSPs are on average 0.14-0.25°C warmer than their corresponding RCPs. Considering the high sensitivity of global and regional glacier mass loss to small temperature increases revealed by our study, the higher warming sensitivity of the SSPs will significantly impact the projected glacier contribution to sea-level rise as well as the number of glaciers anticipated to be lost.

Summary and way forward

Our projections reveal a strong linear relationship between global mean temperature increase and glacier mass loss, with the smallest glacierized regions having a nonlinear relationship beyond +3°C as they experience near complete deglaciation. This strong relationship at global and regional scales, highlights that every increase in temperature has significant consequences with respect to glacier contribution to sea-level rise, the loss of glaciers around the world, and changes to hydrology, ecology, and natural hazards. Regardless of the temperature change scenario, all regions will experience considerable deglaciation at local scales with roughly half of the world's glaciers, by number, projected to be lost by 2100 even if temperature increase is limited to +1.5°C. Based on the most recent climate pledges from COP26, global mean temperature is estimated to increase by +2.7°C (*31*), which would result in much greater glacier contribution to sea-level rise (115±40 mm SLE) and the near complete deglaciation of entire regions including Central Europe, Western Canada and US, and New Zealand (Figs. 5, S11-13) compared to the Paris Agreement. The rapidly increasing glacier mass losses as global temperature increases beyond +1.5°C stresses the urgency of establishing more ambitious climate pledges to preserve these glacierized regions.

References

1. R. Hugonnet, R. McNabb, E. Berthier, B. Menounos, C. Nuth, L. Girod, D. Farinotti, M. Huss, I. Dussaillant, F. Brun, A. Kääb, Accelerated global glacier mass loss in the early twenty-first century. *Nature*. **592**, 726–731 (2021).

2. B. Marzeion, R. Hock, B. Anderson, A. Bliss, N. Champollion, K. Fujita, M. Huss, W. W. Immerzeel, P. Kraaijenbrink, J. H. Malles, F. Maussion, V. Radić, D. R. Rounce, A. Sakai, S. Shannon, R. van de Wal, H. Zekollari, Partitioning the Uncertainty of Ensemble Projections of Global Glacier Mass Change. *Earths Future*. **8** (2020), doi:10.1029/2019EF001470.
3. W. W. Immerzeel, A. F. Lutz, M. Andrade, A. Bahl, H. Biemans, T. Bolch, S. Hyde, S. Brumby, B. J. Davies, A. C. Elmore, A. Emmer, M. Feng, A. Fernández, U. Haritashya, J. S. Kargel, M. Koppes, P. D. A. Kraaijenbrink, A. v. Kulkarni, P. A. Mayewski, S. Nepal, P. Pacheco, T. H. Painter, F. Pellicciotti, H. Rajaram, S. Rupper, A. Sinisalo, A. B. Shrestha, D. Viviroli, Y. Wada, C. Xiao, T. Yao, J. E. M. Baillie, Importance and vulnerability of the world's water towers. *Nature*. **577**, 364–369 (2020).
4. M. Huss, R. Hock, Global-scale hydrological response to future glacier mass loss. *Nat Clim Chang*. **8**, 135–140 (2018).
5. S. Harrison, J. S. Kargel, C. Huggel, J. Reynolds, D. H. Shugar, R. A. Betts, A. Emmer, N. Glasser, U. K. Haritashya, J. Klimeš, L. Reinhardt, Y. Schaub, A. Wiltshire, D. Regmi, V. Vilímek, Climate change and the global pattern of moraine-dammed glacial lake outburst floods. *Cryosphere*. **12**, 1195–1209 (2018).
6. T. L. Edwards, S. Nowicki, B. Marzeion, R. Hock, H. Goelzer, H. Seroussi, N. C. Jourdain, D. A. Slater, F. E. Turner, C. J. Smith, C. M. McKenna, E. Simon, A. Abe-Ouchi, J. M. Gregory, E. Larour, W. H. Lipscomb, A. J. Payne, A. Shepherd, C. Agosta, P. Alexander, T. Albrecht, B. Anderson, X. Asay-Davis, A. Aschwanden, A. Barthel, A. Bliss, R. Calov, C. Chambers, N. Champollion, Y. Choi, R. Cullather, J. Cuzzone, C. Dumas, D. Felikson, X. Fettweis, K. Fujita, B. K. Galton-Fenzi, R. Gladstone, N. R. Golledge, R. Greve, T. Hattermann, M. J. Hoffman, A. Humbert, M. Huss, P. Huybrechts, W. Immerzeel, T. Kleiner, P. Kraaijenbrink, S. le clec'h, V. Lee, G. R. Leguy, C. M. Little, D. P. Lowry, J. H. Malles, D. F. Martin, F. Maussion, M. Morlighem, J. F. O'Neill, I. Nias, F. Pattyn, T. Pelle, S. F. Price, A. Quiquet, V. Radić, R. Reese, D. R. Rounce, M. Rückamp, A. Sakai, C. Shafer, N. J. Schlegel, S. Shannon, R. S. Smith, F. Straneo, S. Sun, L. Tarasov, L. D. Trusel, J. van Breedam, R. van de Wal, M. van den Broeke, R. Winkelmann, H. Zekollari, C. Zhao, T. Zhang, T. Zwinger, Projected land ice contributions to twenty-first-century sea level rise. *Nature*. **593**, 74–82 (2021).
7. F. Maussion, A. Butenko, N. Champollion, M. Dusch, J. Eis, K. Fourteau, P. Gregor, A. H. Jarosch, J. Landmann, F. Oesterle, B. Recinos, T. Rothenpieler, A. Vlug, C. T. Wild, B. Marzeion, The Open Global Glacier Model (OGGM) v1.1. *Geosci Model Dev*. **12**, 909–931 (2019).
8. M. Huss, R. Hock, A new model for global glacier change and sea-level rise. *Front Earth Sci (Lausanne)*. **3** (2015), doi:10.3389/feart.2015.00054.
9. R. Hock, A. Bliss, B. E. N. Marzeion, R. H. Giesen, Y. Hirabayashi, M. Huss, V. Radic, A. B. A. Slangen, GlacierMIP-A model intercomparison of global-scale glacier mass-balance models and projections. *Journal of Glaciology*. **65**, 453–467 (2019).
10. B. Osmanoğlu, M. Braun, R. Hock, F. J. Navarro, Surface velocity and ice discharge of the ice cap on King George Island, Antarctica. *Ann Glaciol*. **54**, 111–119 (2013).
11. B. Osmanoglu, F. J. Navarro, R. Hock, M. Braun, M. I. Corcuera, Surface velocity and mass balance of Livingston Island ice cap, Antarctica. *Cryosphere*. **8**, 1807–1823 (2014).
12. M. Minowa, M. Schaefer, S. Sugiyama, D. Sakakibara, P. Skvarca, Frontal ablation and mass loss of the Patagonian icefields. *Earth Planet Sci Lett*. **561**, 116811 (2021).
13. W. Kochtitzky, L. Copland, W. van Wychen, R. Hugonnet, R. Hock, J. A. Dowdeswell, T. Benham, T. Strozzi, A. Glazovsky, I. Lavrentiev, D. R. Rounce, R. Millan, A. Cook, A.

Dalton, H. Jiskoot, J. Cooley, J. Jania, F. Navarro, The unquantified mass loss of Northern Hemisphere marine-terminating glaciers from 2000–2020. *Nat Commun*. **13**, 5835 (2022).

14. D. R. Rounce, T. Khurana, M. B. Short, R. Hock, D. E. Shean, D. J. Brinkerhoff, Quantifying parameter uncertainty in a large-scale glacier evolution model using Bayesian inference: Application to High Mountain Asia. *Journal of Glaciology*. **66** (2020), doi:10.1017/jog.2019.91.
15. D. R. Rounce, R. Hock, D. E. Shean, Glacier Mass Change in High Mountain Asia Through 2100 Using the Open-Source Python Glacier Evolution Model (PyGEM). *Front Earth Sci (Lausanne)*. **7** (2020), doi:10.3389/feart.2019.00331.
16. K. Hutter, The Effect of Longitudinal Strain on the Shear Stress of an Ice Sheet: In Defence of Using Stretched Coordinates. *Journal of Glaciology*. **27**, 39–56 (1981).
17. D. R. Rounce, R. Hock, R. W. McNabb, R. Millan, C. Sommer, M. H. Braun, P. Malz, F. Maussion, J. Mouginot, T. C. Seehaus, D. E. Shean, Distributed Global Debris Thickness Estimates Reveal Debris Significantly Impacts Glacier Mass Balance. *Geophys Res Lett*. **48** (2021), doi:10.1029/2020GL091311.
18. D. Farinotti, M. Huss, J. J. Fürst, J. Landmann, H. Machguth, F. Maussion, A. Pandit, A consensus estimate for the ice thickness distribution of all glaciers on Earth. *Nat Geosci*. **12**, 168–173 (2019).
19. R. Hock, G. Rasul, C. Adler, B. Cáceres, S. Gruber, Y. Hirabayashi, M. Jackson, A. Kääb, S. Kang, S. Kutuzov, A. Milner, U. Molau, S. Morin, B. Orlove, H. Steltzer, "High Mountain Areas" in *IPCC Special Report on the Ocean and Cryosphere in a Changing Climate*, H.-O. Pörtner, D. C. Roberts, V. Masson-Delmotte, P. Zhai, M. Tignor, E. Poloczanska, K. Mintenbeck, A. Alegría, M. Nicolai, A. Okem, J. Petzold, B. Rama, N. M. Weyer, Eds. (2019).
20. H. Zekollari, M. Huss, D. Farinotti, Modelling the future evolution of glaciers in the European Alps under the EURO-CORDEX RCM ensemble. *Cryosphere*. **13**, 1125–1146 (2019).
21. F. Pithan, T. Mauritsen, Arctic amplification dominated by temperature feedbacks in contemporary climate models. *Nat Geosci*. **7**, 181–184 (2014).
22. J. Bolibar, A. Rabatel, I. Gouttevin, H. Zekollari, C. Galiez, Nonlinear sensitivity of glacier mass balance to future climate change unveiled by deep learning. *Nat Commun*. **13** (2022), doi:10.1038/s41467-022-28033-0.
23. RGI Consortium, “Randolph glacier inventory - A dataset of global glacier outlines: Version 6.0” (2017), , doi:10.7265/N5-RGI-60.
24. D. Scherler, H. Wulf, N. Gorelick, Global Assessment of Supraglacial Debris-Cover Extents. *Geophys Res Lett*. **45**, 11798–11805 (2018).
25. S. Herreid, F. Pellicciotti, The state of rock debris covering Earth’s glaciers. *Nat Geosci*. **13**, 621–627 (2020).
26. G. Østrem, Ice melting under a thin layer of moraine, and the existence of ice cores in moraine ridges. *Geografiska Annaler*. **41**, 228–230 (1959).
27. D. I. Benn, T. Bolch, K. Hands, J. Gulley, A. Luckman, L. I. Nicholson, D. Quincey, S. Thompson, R. Toumi, S. Wiseman, Response of debris-covered glaciers in the Mount Everest region to recent warming, and implications for outburst flood hazards. *Earth Sci Rev*. **114** (2012), pp. 156–174.
28. A. v Rowan, D. L. Egholm, D. J. Quincey, B. Hubbard, O. King, E. S. Miles, K. E. Miles, J. Hornsey, The Role of Differential Ablation and Dynamic Detachment in Driving Accelerating Mass Loss From a Debris-Covered Himalayan Glacier. *J Geophys Res Earth Surf*. **126** (2021), doi:10.1029/2020JF005761.

29. K. B. Tokarska, M. B. Stolpe, S. Sippel, E. M. Fischer, C. J. Smith, F. Lehner, R. Knutti, "Past warming trend constrains future warming in CMIP6 models" (2020), (available at http://advances.sciencemag.org/).
30. K. Wyser, E. Kjellström, T. Koenigk, H. Martins, R. Döscher, Warmer climate projections in EC-Earth3-Veg: The role of changes in the greenhouse gas concentrations from CMIP5 to CMIP6. *Environmental Research Letters*. **15** (2020), doi:10.1088/1748-9326/ab81c2.
31. UNEP, "Emissions Gap Report 2021: The Heat is On - A World of Climate Promises Not Yet Delivered" (Nairobi, 2021), (available at https://www.unep.org/emissions-gap-report-2021).
32. WGMS, "Fluctuations of Glaciers Database" (Zurich, Switzerland, 2021), , doi:10.5904/wgms-fog-2021-05.
33. H. Hersbach, B. Bell, P. Berrisford, S. Hirahara, A. Horányi, J. Muñoz-Sabater, J. Nicolas, C. Peubey, R. Radu, D. Schepers, A. Simmons, C. Soci, S. Abdalla, X. Abellan, G. Balsamo, P. Bechtold, G. Biavati, J. Bidlot, M. Bonavita, G. de Chiara, P. Dahlgren, D. Dee, M. Diamantakis, R. Dragani, J. Flemming, R. Forbes, M. Fuentes, A. Geer, L. Haimberger, S. Healy, R. J. Hogan, E. Hólm, M. Janisková, S. Keeley, P. Laloyaux, P. Lopez, C. Lupu, G. Radnoti, P. de Rosnay, I. Rozum, F. Vamborg, S. Villaume, J. N. Thépaut, The ERA5 global reanalysis. *Quarterly Journal of the Royal Meteorological Society*. **146**, 1999–2049 (2020).
34. P. A. Arias, N. Bellouin, E. Coppola, R. G. Jones, G. Krinner, J. Marotzke, V. Naik, M. D. Palmer, G.-K. Plattner, J. Rogelj, M. Rojas, J. Sillmann, T. Storelvmo, P. W. Thorne, B. Trewin, K. Achuta Rao, B. Adhikary, R. P. Allan, K. Armour, G. Bala, R. Barimalala, S. Berger, J. G. Canadell, C. Cassou, A. Cherchi, W. Collins, W. D. Collins, S. L. Connors, S. Corti, F. Cruz, F. J. Dentener, C. Dereczynski, A. di Luca, A. Diongue Niang, F. J. Doblas-Reyes, A. Dosio, H. Douville, F. Engelbrecht, V. Eyring, E. Fischer, P. Forster, B. Fox-Kemper, J. S. Fuglestvedt, J. C. Fyfe, N. P. Gillet, L. Goldfarb, I. Gorodetskaya, J. M. Gutierrez, R. Hamdi, E. Hawkins, H. T. Heewitt, P. Hope, A. S. Islam, C. Jones, D. S. Kaufman, R. E. Kopp, Y. Kosaka, J. Kossin, S. Krakovska, J.-Y. Lee, J. Li, T. Mauritsen, T. K. Maycock, M. Meinshausen, S.-K. Min, P. M. S. Monteiro, T. Ngo-Duc, F. Otto, I. Pinto, A. Pirani, K. Raghavan, R. Ranasinghe, A. C. Ruane, L. Ruiz, J.-B. Sallée, B. H. Samset, S. Sathyendranath, S. I. Seneviratne, A. A. Sörensson, S. Szopa, I. Takayabu, A.-M. Trguier, B. van den Hurk, R. Vautard, K. von Schuckmann, S. Zaehle, X. Zhang, K. Zickfeld, "Technical Summary" in *Climate Change 2021: The Physical Science Basis. Contribution of Working Group 1 to the Sixth Assessment Report of the Intergovernmental Panel on Climate Change*, V. Masson-Delmotte, P. Zhai, A. Pirani, S. L. Connors, C. Péan, S. Berger, N. Caud, Y. Chen, L. Goldfarb, M. I. Gomis, M. Huang, K. Leitzell, E. Lonnoy, J. B. R. Matthews, T. K. Maycock, T. Waterfield, O. Yelekci, R. Yu, B. Zhou, Eds. (Cambridge University Press, 2021).
35. J. Oerlemans, F. M. Nick, A minimal model of a tidewater glacier. *Ann Glaciol*. **42**, 1–6 (2005).
36. J. G. Cogley, R. Hock, L. A. Rasmussen, A. A. Arendt, A. Bauder, R. J. Braithwaite, P. Jansso, G. Kaser, M. Möller, L. Nicholson, M. Zemp, "Glossary of Glacier Mass Balance and Related Terms" (Paris, 2011).
37. C. E. Rasmussen, C. K. I. Williams, *Gaussian Processes for Machine Learning* (MIT Press, Cambridge, MA, 2006).
38. D. P. Kingma, J. Ba, Adam: A Method for Stochastic Optimization (2014) (available at http://arxiv.org/abs/1412.6980).

39. R. J. Braithwaite, Temperature and precipitation climate at the equilibrium-line altitude of glaciers expressed by the degree-day factor for melting snow. *Journal of Glaciology*. **54**, 437–444 (2008).
40. R. Millan, J. Mouginot, A. Rabatel, M. Morlighem, Ice velocity and thickness of the world's glaciers. *Nat Geosci*. **15**, 124–129 (2022).
41. B. Recinos, F. Maussion, T. Rothenpieler, B. Marzeion, Impact of frontal ablation on the ice thickness estimation of marine-terminating glaciers in Alaska. *Cryosphere*. **13**, 2657–2672 (2019).

Acknowledgments: This work was supported in part by the high-performance computing and data storage resources operated by the Research Computing Systems Group at the University of Alaska Fairbanks Geophysical Institute. This text reflects only the author's view and funding agencies are not responsible for any use that may be made of the information it contains.

Funding:

National Aeronautics and Space Administration grant 80NSSC20K1296 (DR, ReHo)

National Aeronautics and Space Administration grant 80NSSC20K1595 (DR, ReHo)

National Aeronautics and Space Administration grant 80NSSC17K0566 (DR, ReHo)

National Aeronautics and Space Administration grant NNX17AB27G (DR, ReHo)

Norwegian Research Council project #324131 (ReHo)

Tula Foundation and Canada Research Chairs (BM)

National Sciences and Engineering Research Council of Canada (BM, LuCo)

Vanier Graduate Scholarship (WK)

Swiss National Science Foundation project nr. 184634 (RoHu, MH, LoCo, DF)

ArcticNet Network of Centres of Excellence Canada (LuCo)

University of Ottawa, University Research Chair program (LuCo)

European Union's Horizon 2020 research and innovation programme grant 101003687 (FM)

Austrian Science Fund (FWF) grant P30256 (FM)

French Space Agency CNES (EB, RoHu)

Author contributions:

Conceptualization: DR, ReHo

Data curation: DR

Formal analysis: DR

Funding acquisition: DR, ReHo, MH, DF, EB, BM, LuCo

Investigation: DR

Methodology: DR, FM, ReHo

Project administration: DR, ReHo

Resources: DR, FM (glacier data); RoHu, MH, EB, DF, BM, and RM (mass balance data); LoCo (climate data); WK and LuCo (frontal ablation data)

Software: DR (PyGEM); FM (OGGM); DB (emulators)

Visualization: DR, ReHo

Writing – original draft: DR

Writing – review & editing: all authors, especially ReHo

Competing interests: Authors declare that they have no competing interests.

Data and materials availability: The datasets generated for this study can be found in the National Snow & Ice Data Center (NSIDC) following acceptance. During the review process, the data will be publicly available at https://drive.google.com/drive/folders/1VXLkBxnj521j6HHy6RUFerqgiZGxMNqG?usp=sharing. The model code is publicly available at https://github.com/drounce/PyGEM and https://github.com/OGGM/ogggm.

Supplementary Materials

Methods

References (*32–41*)

Figs. S1 to S28

Tables S1 to S5

Science
AAAS

Supplementary Materials for

Global glacier change in the 21st century: Every increase in temperature matters

David R. Rounce, Regine Hock, Fabien Maussion, Romain Hugonnet, William Kochtitzky, Matthias Huss, Etienne Berthier, Douglas Brinkerhoff, Loris Compagno, Luke Copland, Daniel Farinotti, Brian Menounos, Robert W. McNabb

Correspondence to: drounce@cmu.edu

This PDF file includes:

Methods

Glacier data

Glacier outlines of all ~215,000 glaciers covering an area of 705,739 km^2 are provided by the Randolph Glacier Inventory (RGI, version 6) (*23*). Glacier-wide geodetic mass change rates for each glacier from 2000 to 2019 (*1*) are used for model calibration. Frontal ablation data from 2000 to 2020 in the Northern Hemisphere (*13*), South America (*12*), and Antarctica (*10*, *11*) are used to calibrate marine-terminating glaciers. Annual and seasonal glaciological glacier-wide mass balance data from 1979 to 2019 (*32*) are used for model validation (Figs. S23-26). Spatially distributed sub-debris melt enhancement factors for all debris-covered glaciers (*17*) are used to account for the enhanced or suppressed melting due to debris thickness. The Open Global Glacier Model (OGGM) (*7*) was used to compile these data sets with a digital elevation model for each glacier to bin the data according to the glacier central flowlines. OGGM is also used to estimate each glacier´s initial ice thickness, while ensuring that each region´s total glacier volume matches the regional multi-model ice thickness estimates (*18*) (see Model calibration).

Climate data

Monthly near-surface air temperature and precipitation data from ERA5 (*33*) are used for historical (1980-2019) simulations. Air temperature lapse rates are estimated using monthly air temperature data from various pressure levels.

An ensemble of ten GCMs and three RCPs (RCP2.6, RCP4.5, and RCP8.5), i.e., the same as those used by GlacierMIP (*2*), and an ensemble of 12 GCMs forced by four SSPs (SSP1-2.6, SSP2-4.5, SSP3-7.0, and SSP5-8.5) are used for the projections (Table S3). Future simulations are adjusted using additive factors for air temperature and multiplicative factors for precipitation to remove any bias between the GCMs and ERA5 data over the calibration period (2000-2019) (*14*, *15*).

Following the Intergovernmental Panel on Climate Change (*34*), mean global temperature change from 2081-2100 compared to pre-industrial levels is computed by adding the observed increase of +0.63°C from 1850-1900 until 1986-2005 to each GCM´s projected temperature increase between 1986-2005 and 2081-2100. Four GCMs also provided data for SSP1-1.9, which are used to provide additional forcing for low mean global temperature change scenarios. Projections are aggregated into +1.5°C, +2°C, +3°C, and +4°C temperature change scenarios based on the global mean temperature change for each combination of GCM and emission scenario with a tolerance of ±0.25 for the 1.5°C scenario and ±0.5 for all others.

Glacier modeling

The glacier evolution model is a hybrid model that uses the mass balance module of the Python Glacier Evolution Model (PyGEM) (*14*, *15*) and the glacier dynamics module from OGGM (*7*) to model every glacier independently from 2000-2100 for various ensembles of GCMs, SSPs, and RCPs. The model computes the climatic mass balance (i.e., snow accumulation minus melt plus refreezing) for each surface elevation bin using a monthly time step. The model computes glacier melt using a degree-day model, accumulation using a temperature threshold, and refreezing based on the annual air temperature (*14*, *15*). Glacier geometry is updated annually using a flowline model based on the Shallow-Ice Approximation to explicitly account for glacier dynamics (*7*) using a density of 900 kg m^{-3} for converting mass to volume. For marine-terminating glaciers, frontal ablation is modeled using a frontal ablation parameterization coupled to the ice dynamical model. Mass is removed at the glacier front when the bedrock is below sea level using an empirical formula (*35*). Mass changes are converted to

sea-level change using an ocean area of 3.625 x 10^8 km^2 (*36*). The glacier contribution to sea-level rise is corrected to account for the effect of grounded ice below sea level displacing ocean water for marine-terminating glaciers (*8*).

Model calibration

The mass balance model uses three parameters, i.e., temperature bias, precipitation factor, and degree-day factor of snow (a ratio of 0.7 between the degree-day factor of snow and ice is used to estimate the factor for ice), that are assumed constant in time. The temperature bias and precipitation factor downscale the GCM data to the glacier-scale, and the degree-day factors control melt rates. Bayesian inference is used to calibrate the three parameters for each glacier based on Markov Chain Monte Carlo (MCMC) methods (*14*, *15*) with geodetic mass balance data from 2000-2019 (*1*) and a mass balance emulator for each glacier. An independent emulator for each glacier was derived by performing 100 present-day simulations based on randomly sampled model parameter sets and then fitting a Gaussian Process to these parameter-response pairs. This model was then substituted for PyGEM within the MCMC sampler, which reduced the computational expense by two orders of magnitude. For all Gaussian process emulators, we use the squared-exponential covariance function, which has hyperparameters controlling the characteristic amplitude and correlation length scale, along with a Gaussian likelihood model (with observation noise hyperparameter) and a constant mean. We optimize hyperparameters by maximizing the marginal log-likelihood (*37*) using the Adam optimizer (*38*).

A comparison of the MCMC methods using the emulator versus full model simulations for a subset of 2500 randomly selected glaciers was performed. The posterior predictive distribution of the mass balance and marginal posterior distributions of the temperature bias, precipitation factor, and degree-day factor of snow agree well, especially for glaciers with an initial area greater than 1 km^2 (Fig. S27). Specifically, 95% of the differences in the median of the posterior predictive distribution for the mass balance are between -0.06 to 0.04 m w.e. yr^{-1}, which is well below the mean uncertainty associated with the geodetic mass balance data (0.27 m w.e. yr^{-1}) (Hugonnet et al. 2021). The differences for the marginal posterior distributions of the temperature bias are -0.45 to 0.64°C, precipitation factor are -0.32 to 0.35, and the degree-day factor of snow are -0.57 to 0.70 mm w.e. d^{-1} $°C^{-1}$. These differences in the marginal distribution are less than the normalized median absolute deviation associated with the full simulation for each parameter (0.86°C for the temperature bias; 0.55 for the precipitation factor; and 1.29 mm w.e. d^{-1} $°C^{-1}$ for the degree-day factor of snow). Given that most glaciers smaller than 1 km^2 are projected to completely disappear regardless of the future climatic forcing, the use of emulators should have minimal impact on the projections.

The prior distributions for the degree-day factor were based on previous data (*39*), while the temperature bias and precipitation factor were derived using a simple optimization scheme (*14*), which provides an approximation of the regional joint prior distribution for each RGI Order 2 subregion. The temperature bias assumes a normal distribution and the precipitation factor assumes a gamma distribution to ensure positivity. Glacier-wide winter mass balance data (*32*) were used to determine a reasonable upper-level constraint for the precipitation factor for the simple optimization scheme.

The glacier dynamics model relies on a single parameter (ice viscosity) that is calibrated at the regional level to match the multi-model ice volume estimates (*18*). The same value is then used for the projections. In future simulations, the initial ice thickness is estimated for each glacier, GCM, scenario, and set of model parameters using a mass-conservation inversion approach (*7*), which enables the simulations to account for uncertainty associated with the initial

ice thickness (Table S4). The uncertainty associated with the initial ice thickness varies regionally ranging from ±2 to ±9%. This range of uncertainty captures most of the regional differences between a recent estimate of ice thickness (*40*) compared to the multi-model "consensus" estimate (*18*) used in our study. In regions where differences are larger (e.g., High Mountain Asia, Greenland Periphery), one can expect the glacier contribution to sea-level to vary by roughly the same percentage as the differences in initial volume (*8*).

Marine-terminating glaciers

Marine-terminating glaciers have an additional frontal ablation parameter that is assumed constant in time and calibrated for each individual glacier to match frontal ablation data (*10–13*) (Fig. S28). The frontal ablation calibration is performed independently of the Bayesian calibration scheme to avoid circularity issues associated with the frontal ablation, climatic mass balance, and ice thickness inversion. The optimization is performed using a bisection method. The initial ice thickness is estimated using the mass balance parameters assuming the glacier is land-terminating. Then a forward simulation from 2000-2019 is run to estimate the frontal ablation. If a dynamic instability error occurs during the forward simulation (8% of glaciers), the glacier dynamics model uses mass redistribution curves instead (*8*, *15*). Uncertainty associated with the frontal ablation parameter is estimated by performing the optimization to match ±1 standard deviation of the frontal ablation data (*10–13*). The frontal ablation parameter is assumed to have a truncated normal distribution based on the mean, standard deviation, and lower and upper bounds of 0.001 and 5 (*8*). For quality control, we combined the frontal ablation and geodetic mass balance observations to estimate climatic mass balances (*36*). For some glaciers, the resulting climatic mass balances are unrealistic due to errors in the RGI outlines and/or poor glacier thickness and velocity data used in frontal ablation calculations. For these glaciers, we assume frontal ablation is overestimated and reduce the frontal ablation to ensure the climatic mass balance is within three standard deviations of the regional mean from the geodetic mass balance data. The Antarctic and Subantarctic region has the sparsest frontal ablation data, so the region's median frontal ablation parameter and corresponding standard deviation is used for glaciers that lack frontal ablation data.

Inclusion of frontal ablation when estimating initial ice thickness increases the mass of ice (*41*), globally by 16% and regionally from less than 1% (Arctic Canada North) to 48% (Antarctic and Subantarctic), compared to excluding frontal ablation. The increase in initial ice thickness primarily occurs at the glacier terminus such that 57% of the additional mass is below sea level. Globally, the percentage of mass below sea level increases from 10% (excluding frontal ablation) to 17% (including frontal ablation) and the initial mass in units of potential sea-level equivalent increases by 23 mm SLE when including frontal ablation.

Model uncertainty

For each GCM and future climate scenario (RCP or SSP), 50 simulations are run based on the posterior distributions from the Bayesian inference to account for model parameter uncertainty. Regional results are derived by aggregating the median of these individual glacier runs and uncertainty is shown as the ensemble median and 95% confidence interval for each scenario. The only exception is the uncertainty associated with the annual frontal ablation rates. Since the frontal ablation parameterization is insensitive to temperature and precipitation forcing and not coupled to an ocean model, the multi-GCM uncertainty underestimates the actual uncertainty. Instead, the 95% confidence interval accompanying the mean annual frontal ablation rate is based on the model parameter uncertainty assuming glacier frontal ablation rates are perfectly correlated within the same region and individual regions are independent.

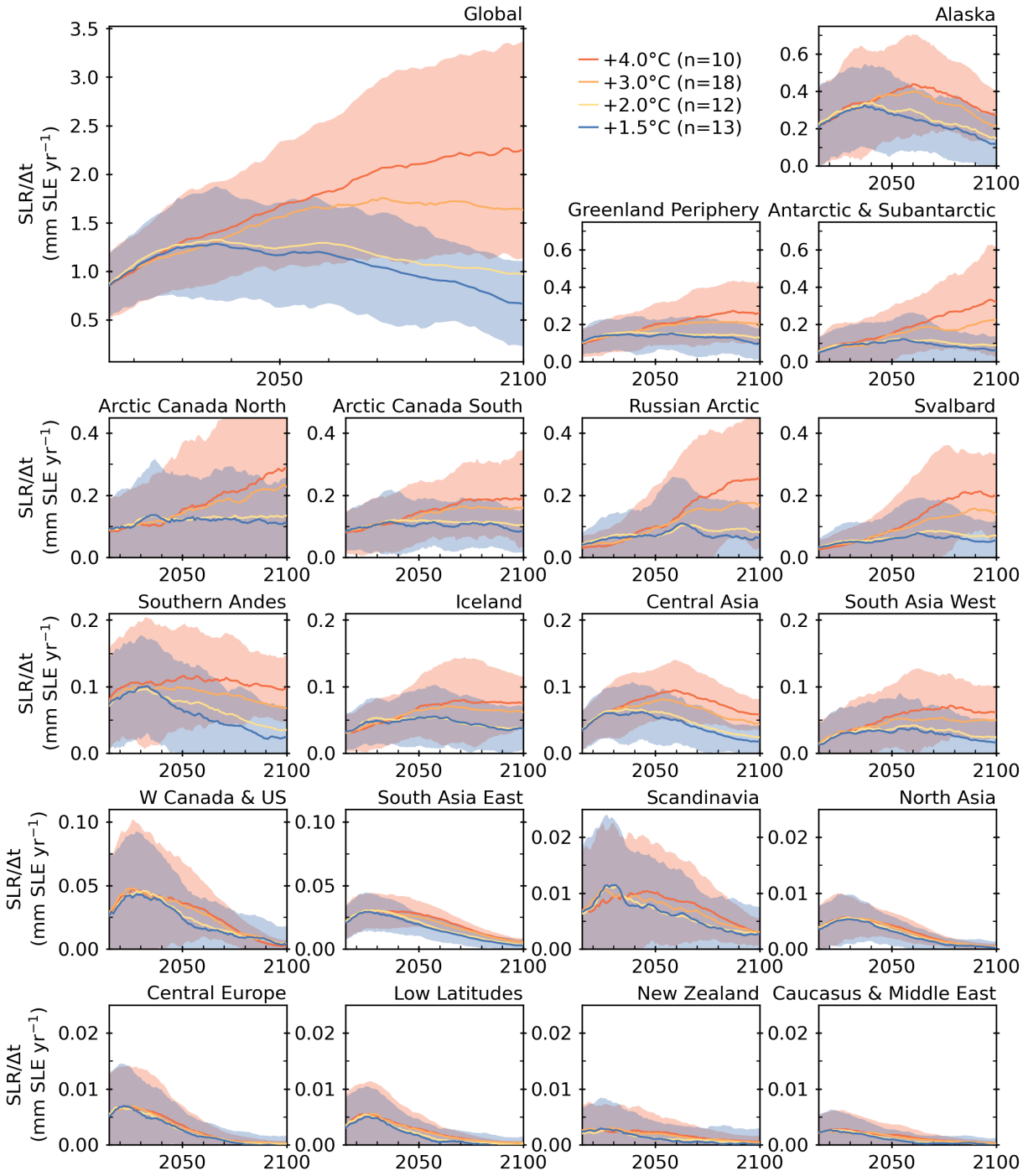

Fig. S1.

Global and regional rates of glacier contribution to sea-level change from 2015 to 2100 for global temperature change scenarios in 2100 relative to pre-industrial levels. Colors depict the ensemble median and shading indicates the 95% confidence interval (shown only for the +1.5°C and +4°C scenarios). The number of glacier projections with different GCMs and SSP scenarios that fall into each temperature change scenario is shown in the legend. Regions are ordered by their total mass loss. Note the scale varies among panels.

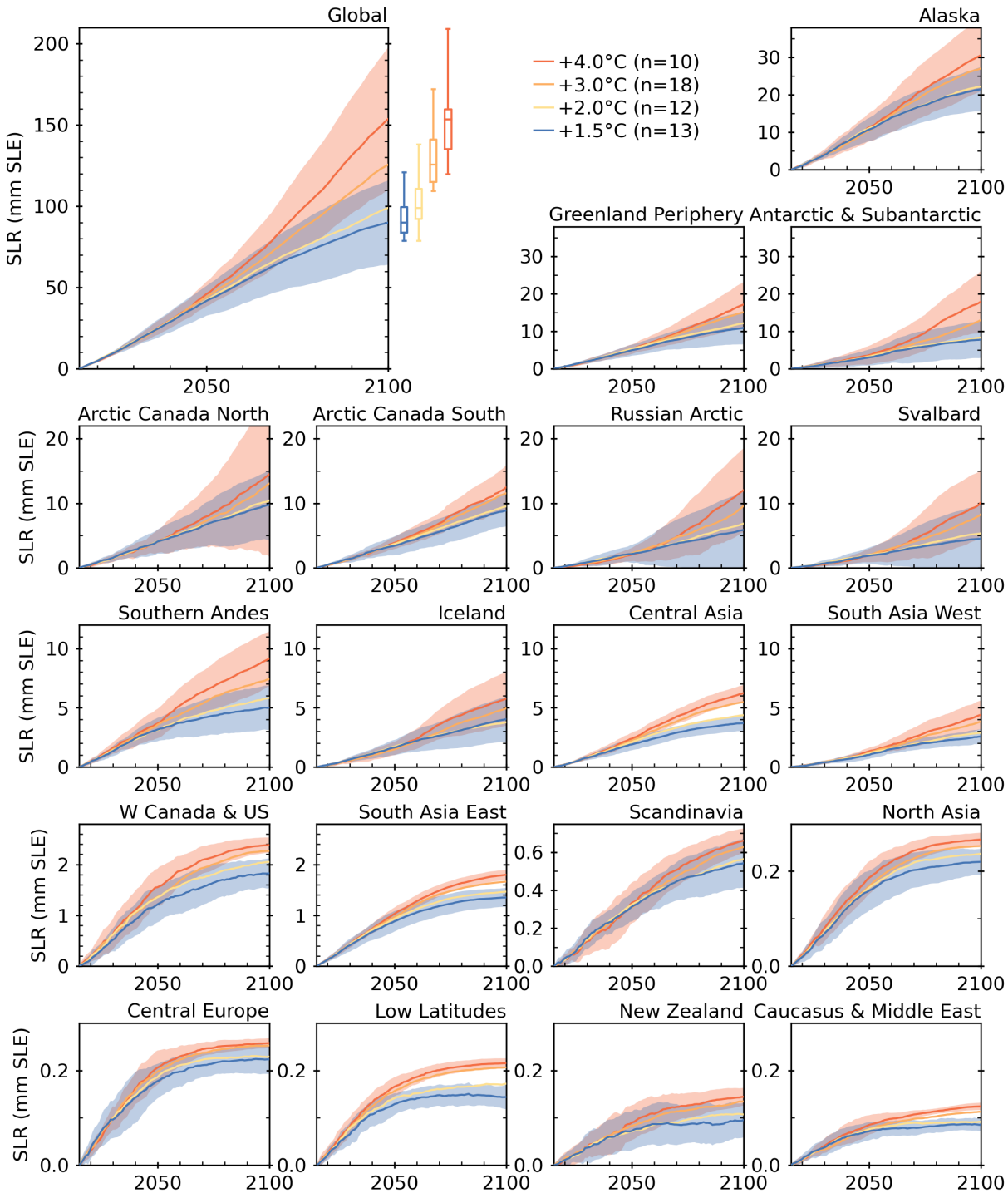

Fig. S2.
Global and regional projections of the cumulative contribution from annual glacier mass change to sea level rise (SLR) from 2015 to 2100 for global temperature change scenarios. Colors depict the ensemble median and shading indicates the 95% confidence interval (shown only for the +1.5°C and +4°C scenarios). The number of glacier projections with different GCMs and SSP scenarios that fall into each temperature change scenario is shown in the legend. Regions are ordered by their total mass loss. Note the scale varies among panels.

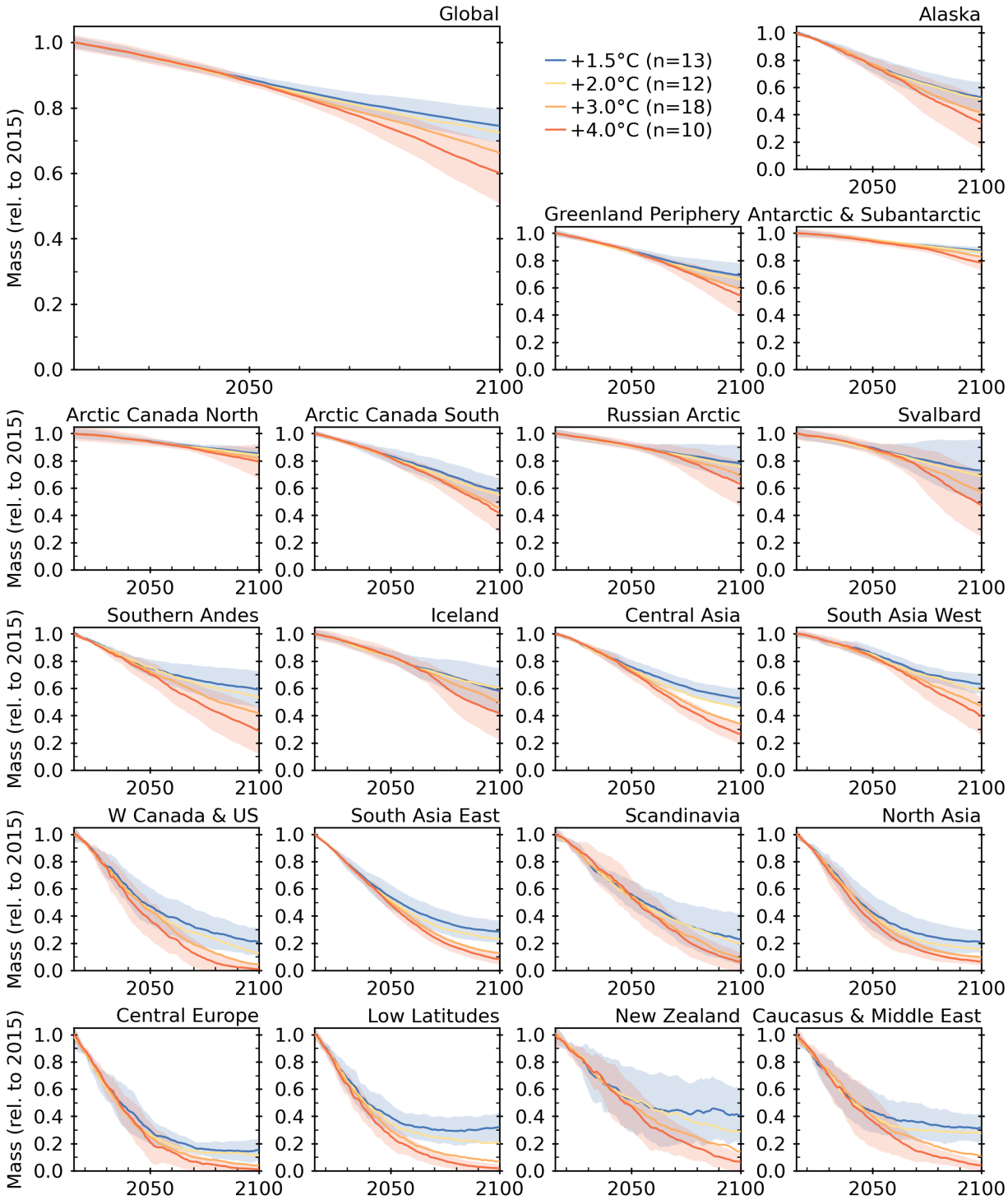

Fig. S3.
Global and regional mass from 2015 to 2100, relative to 2015, for global temperature change scenarios. Colors depict the ensemble median and shading indicates the 95% confidence interval (shown only for the +1.5°C and +4°C scenarios). The number of glacier projections with different GCMs and SSP scenarios that fall into each temperature change scenario is shown in the legend. Regions are ordered by their total mass loss.

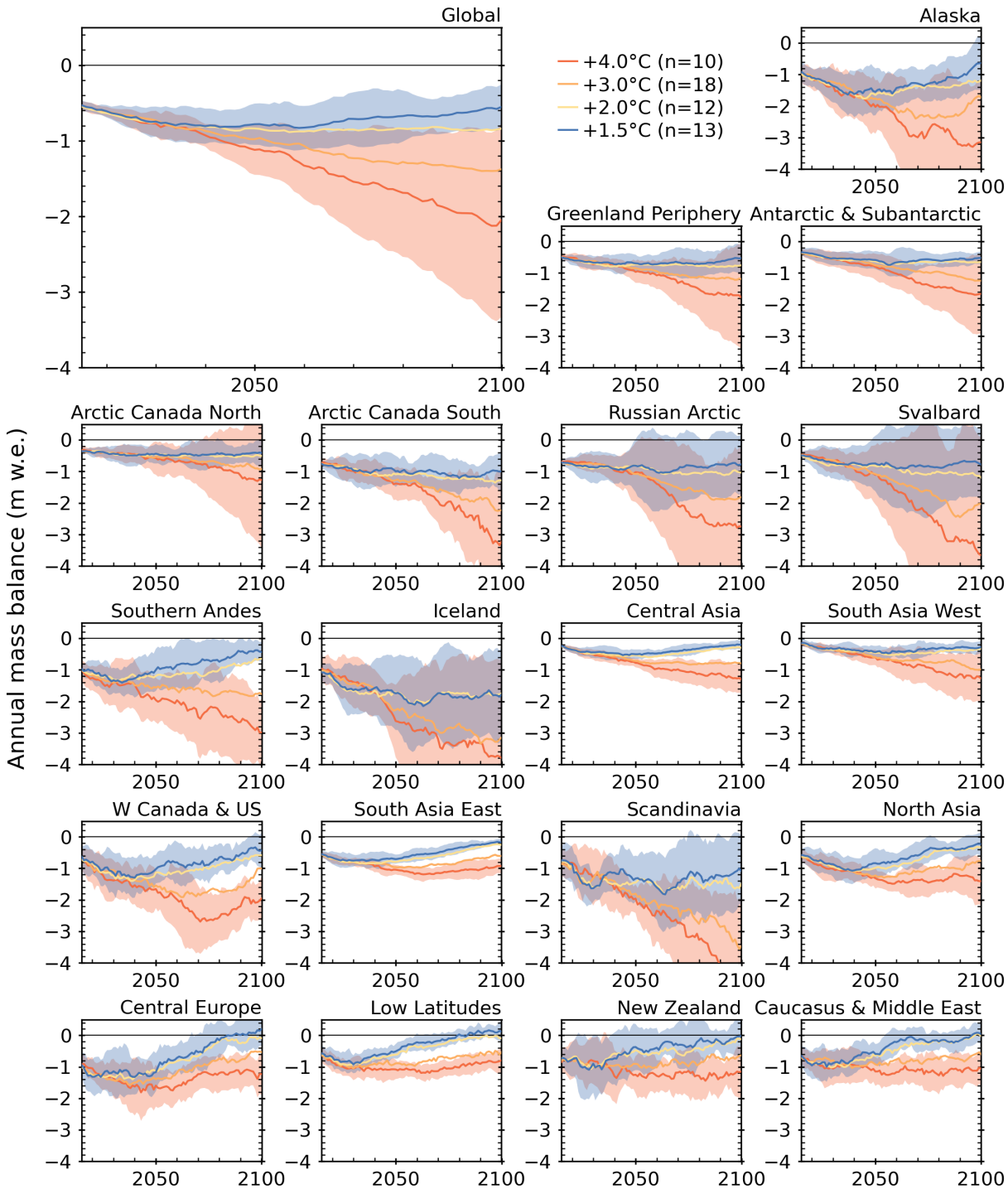

Fig. S4.
Global and regional area-averaged annual glacier mass balance from 2015 to 2100 for global temperature change scenarios in 2100 relative to pre-industrial levels. Colors depict the ensemble median and shading indicates the 95% confidence interval (shown only for the +1.5°C and +4°C scenarios). An 11-year running mean is used to reduce variability in individual years. The number of glacier projections with different GCMs and SSP scenarios that fall into each temperature change scenario is shown in the legend. Regions are ordered by their total mass loss.

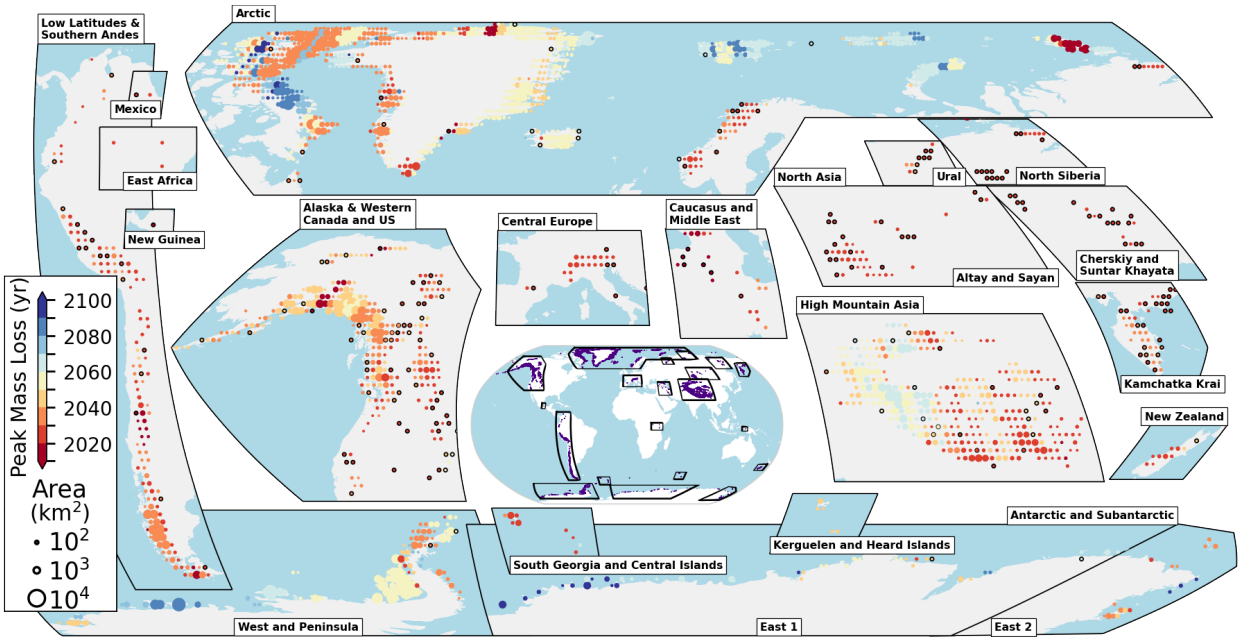

Fig. S5.
Spatial distribution of the year of maximum annual glacier mass loss (Gt) for +1.5°C. Tiles are aggregated by 1°x1° below 60° latitude, 2°x1° between 60° and 74° latitude and 2°x2° above 74° latitude to represent approximately 10,000 km² each. Circles are scaled based on glacierized area in 2015 and are colored by the year of maximum mass loss. Tiles that have experienced complete deglaciation by 2100 are marked by black circles. An 11-year running mean is used to reduce variability in individual years.

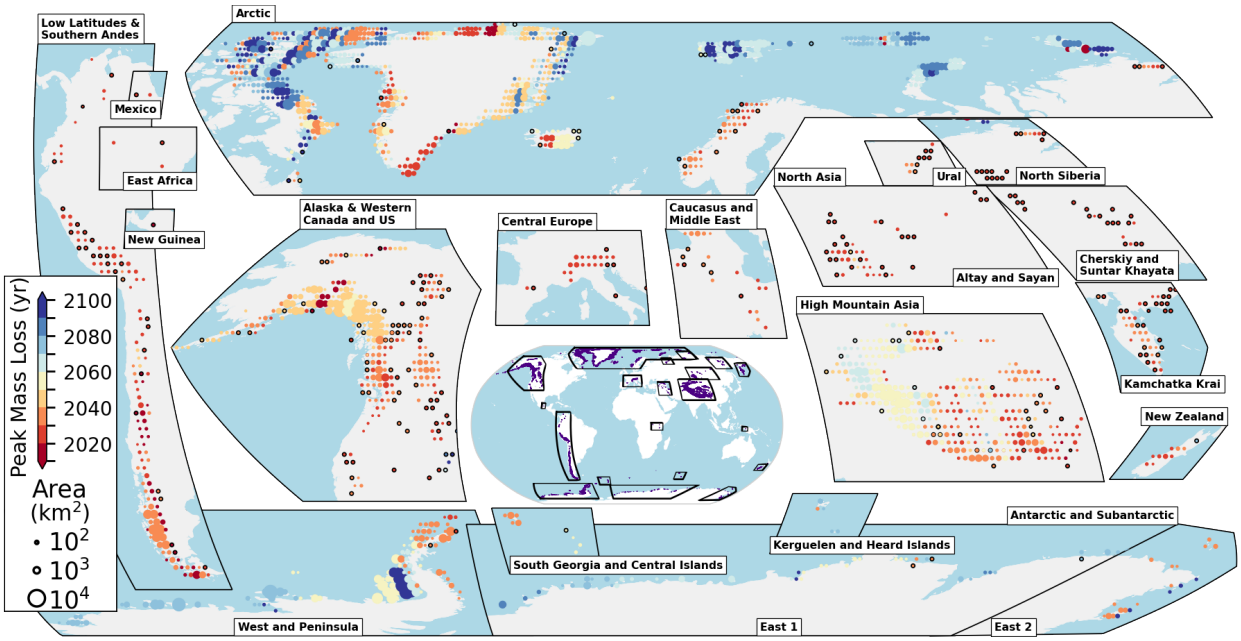

Fig. S6.
Spatial distribution of the year of maximum annual glacier mass loss (Gt) for +2°C. Tiles are aggregated by 1°x1° below 60° latitude, 2°x1° between 60° and 74° latitude and 2°x2° above 74° latitude to represent approximately 10,000 km² each. Circles are scaled based on glacierized area in 2015 and are colored by the year of maximum mass loss. Tiles that have experienced complete deglaciation by 2100 are marked by black circles. An 11-year running mean is used to reduce variability in individual years.

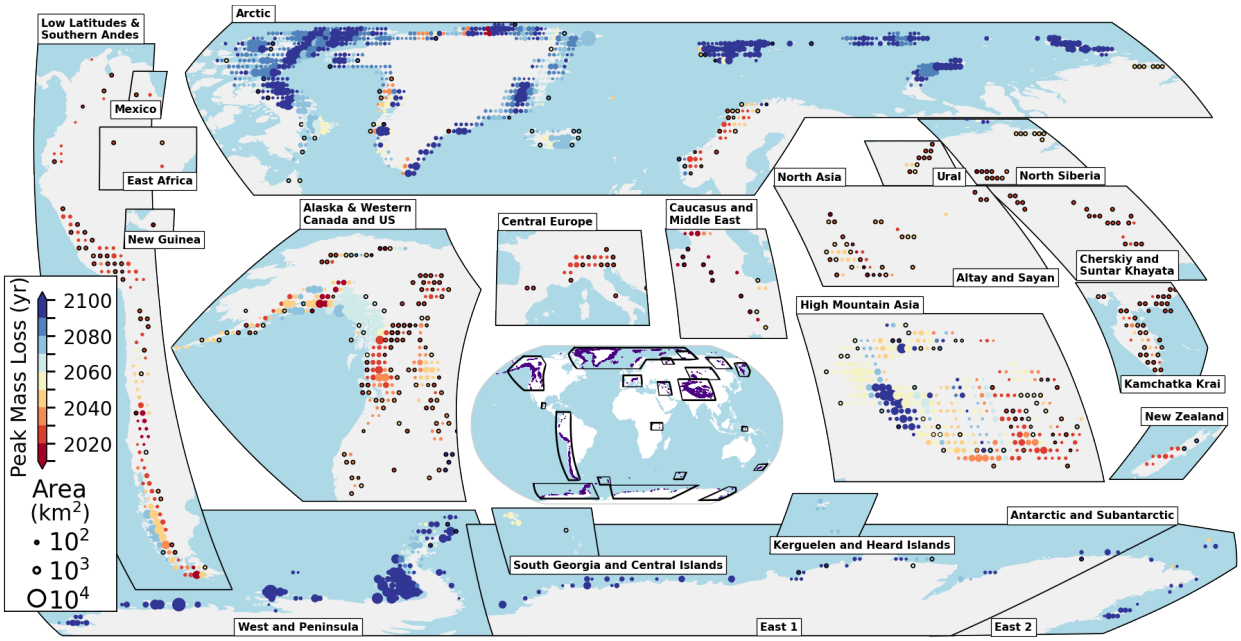

Fig. S7.
Spatial distribution of the year of maximum annual glacier mass loss (Gt) for +3°C. Tiles are aggregated by 1°x1° below 60° latitude, 2°x1° between 60° and 74° latitude and 2°x2° above 74° latitude to represent approximately 10,000 km² each. Circles are scaled based on glacierized area in 2015 and are colored by the year of maximum mass loss. Tiles that have experienced complete deglaciation by 2100 are marked by black circles. An 11-year running mean is used to reduce variability in individual years.

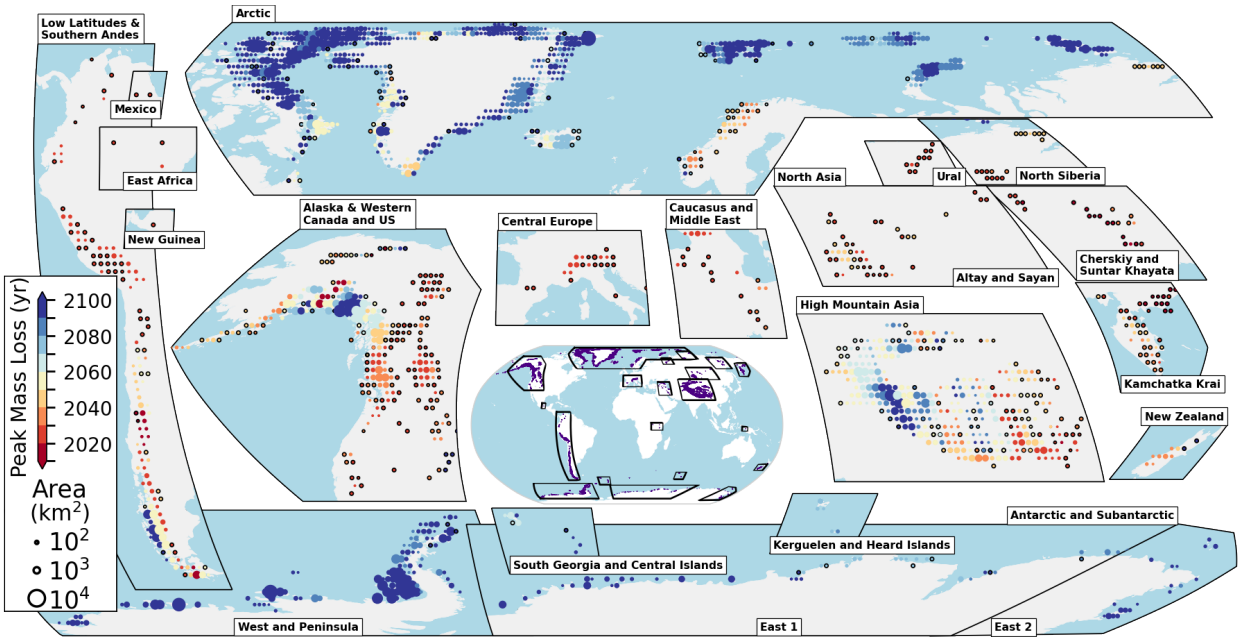

Fig. S8.
Spatial distribution of the year of maximum annual glacier mass loss (Gt) for +4°C. Tiles are aggregated by 1°x1° below 60° latitude, 2°x1° between 60° and 74° latitude and 2°x2° above 74° latitude to represent approximately 10,000 km² each. Circles are scaled based on glacierized area in 2015 and are colored by the year of maximum mass loss. Tiles that have experienced complete deglaciation by 2100 are marked by black circles. An 11-year running mean is used to reduce variability in individual years.

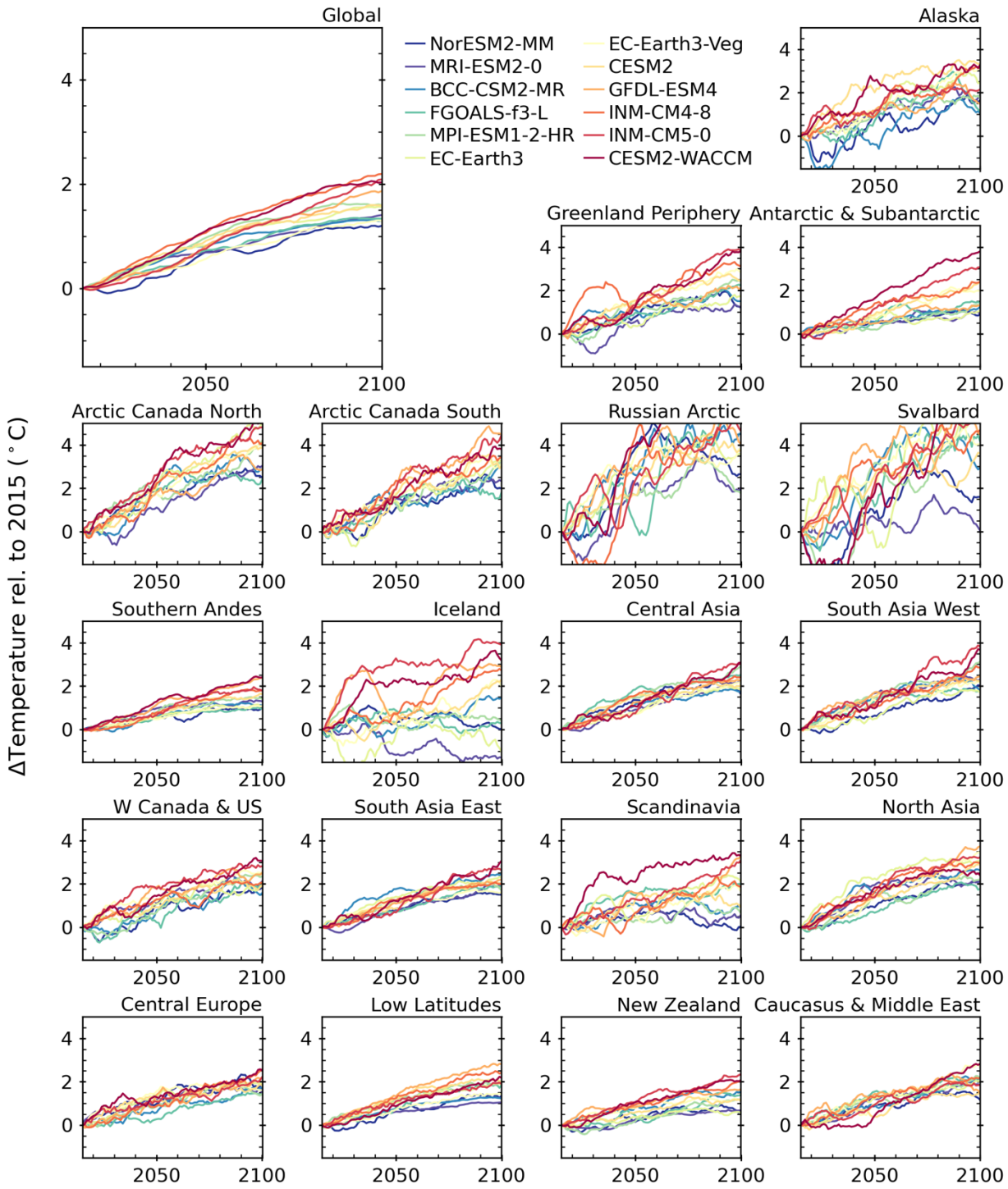

Fig. S9.
Global and regional projections of the annual temperature anomaly for glacierized regions from 2015 to 2100 for SSP2-4.5. Colors depict the GCMs. 11-year running mean used to reduce noise. Regions are ordered by their total mass loss.

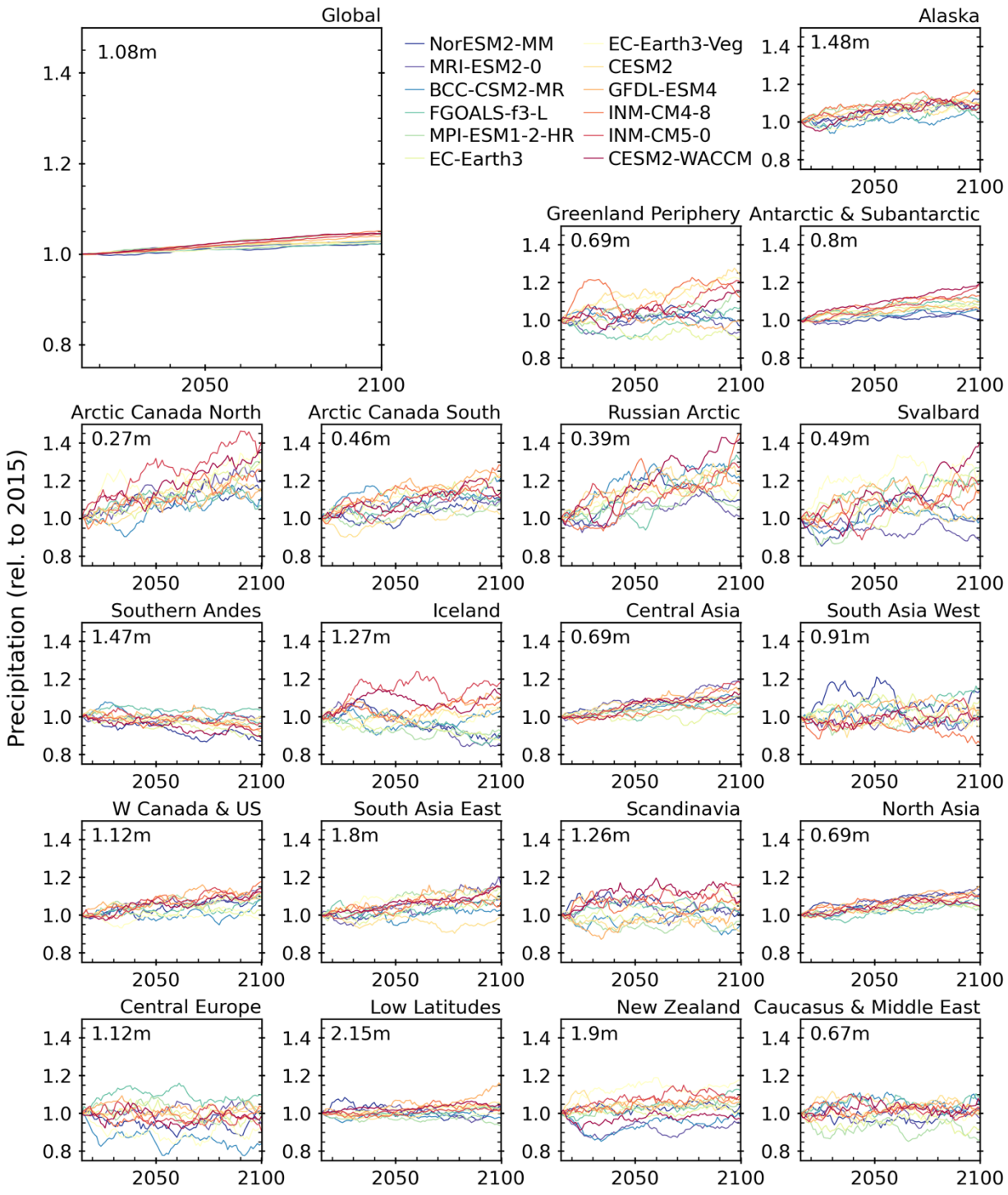

Fig. S10.
Global and regional projections of the annual precipitation anomaly for glacierized regions from 2015 to 2100 for SSP2-4.5. Colors depict the GCMs. 11-year running mean used to reduce noise. Text shows mean precipitation for each region of all GCMs in 2015. Regions are ordered by their total mass loss.

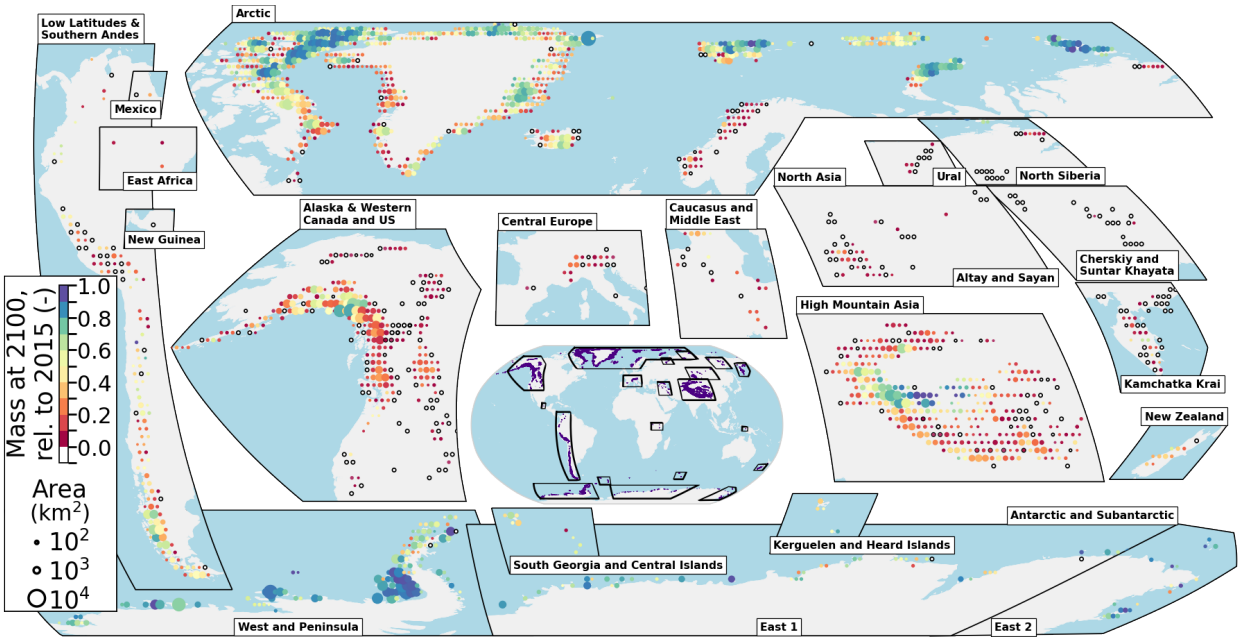

Fig. S11.
Spatial distribution of the ensemble median glacier mass remaining by 2100, relative to 2015, for the +1.5°C scenario. Tiles are aggregated by 1°x1° below 60° latitude, 2°x1° between 60° and 74° latitude and 2°x2° above 74° latitude to represent approximately 10,000 km² each. Circles are scaled based on simulated glacierized area in 2015 and are colored by normalized mass remaining. Tiles that have experienced complete deglaciation by 2100 are shown in white and outlined by a black circle.

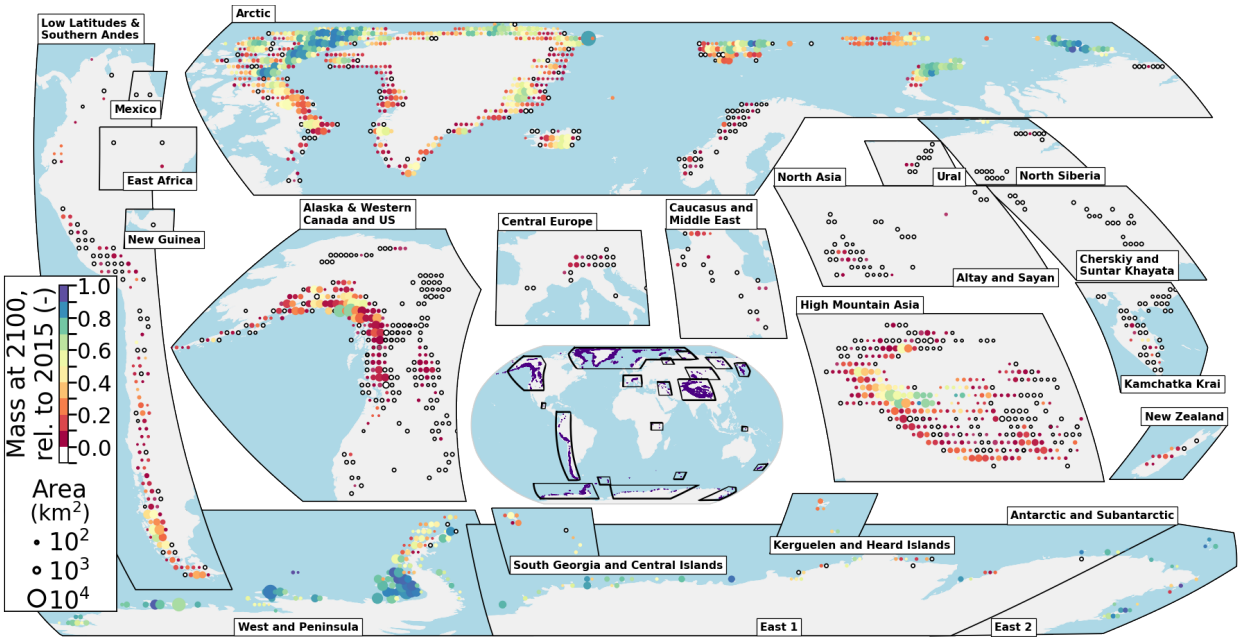

Fig. S12.
Spatial distribution of the ensemble median glacier mass remaining by 2100, relative to 2015, for the +3°C scenario. Tiles are aggregated by 1°x1° below 60° latitude, 2°x1° between 60° and 74° latitude and 2°x2° above 74° latitude to represent approximately 10,000 km² each. Circles are scaled based on simulated glacierized area in 2015 and are colored by normalized mass remaining. Tiles that have experienced complete deglaciation by 2100 are shown in white and outlined by a black circle.

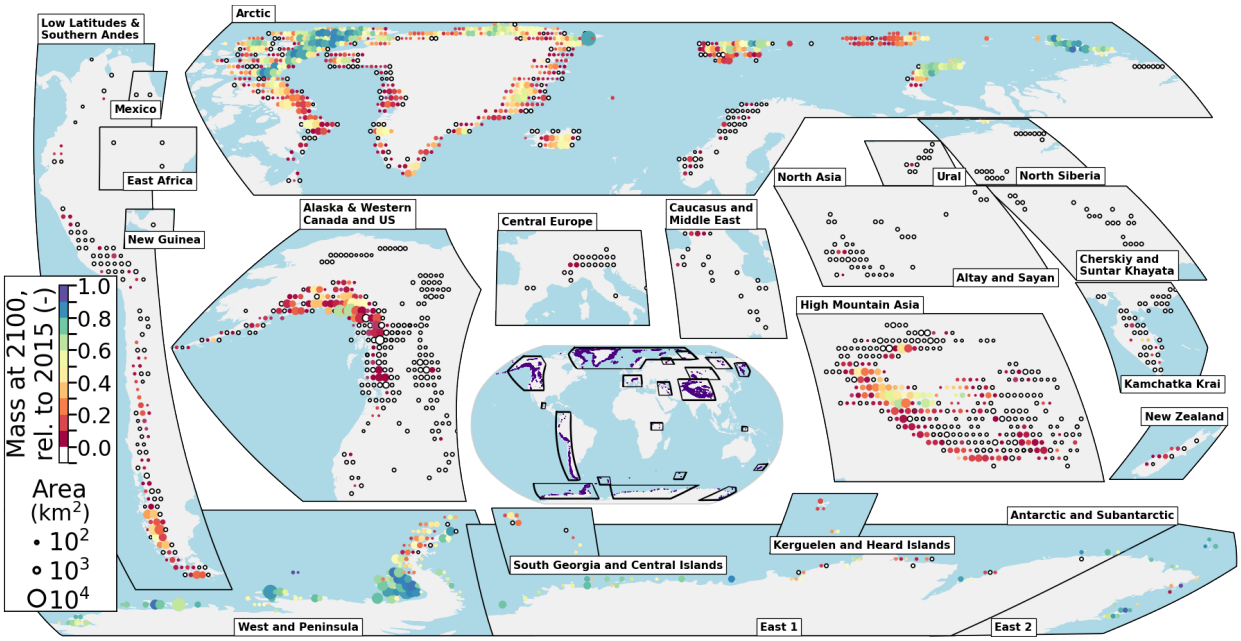

Fig. S13.
Spatial distribution of the ensemble median glacier mass remaining by 2100, relative to 2015, for the +4°C scenario. Tiles are aggregated by 1°x1° below 60° latitude, 2°x1° between 60° and 74° latitude and 2°x2° above 74° latitude to represent approximately 10,000 km² each. Circles are scaled based on simulated glacierized area in 2015 and are colored by normalized mass remaining. Tiles that have experienced complete deglaciation by 2100 are shown in white and outlined by a black circle.

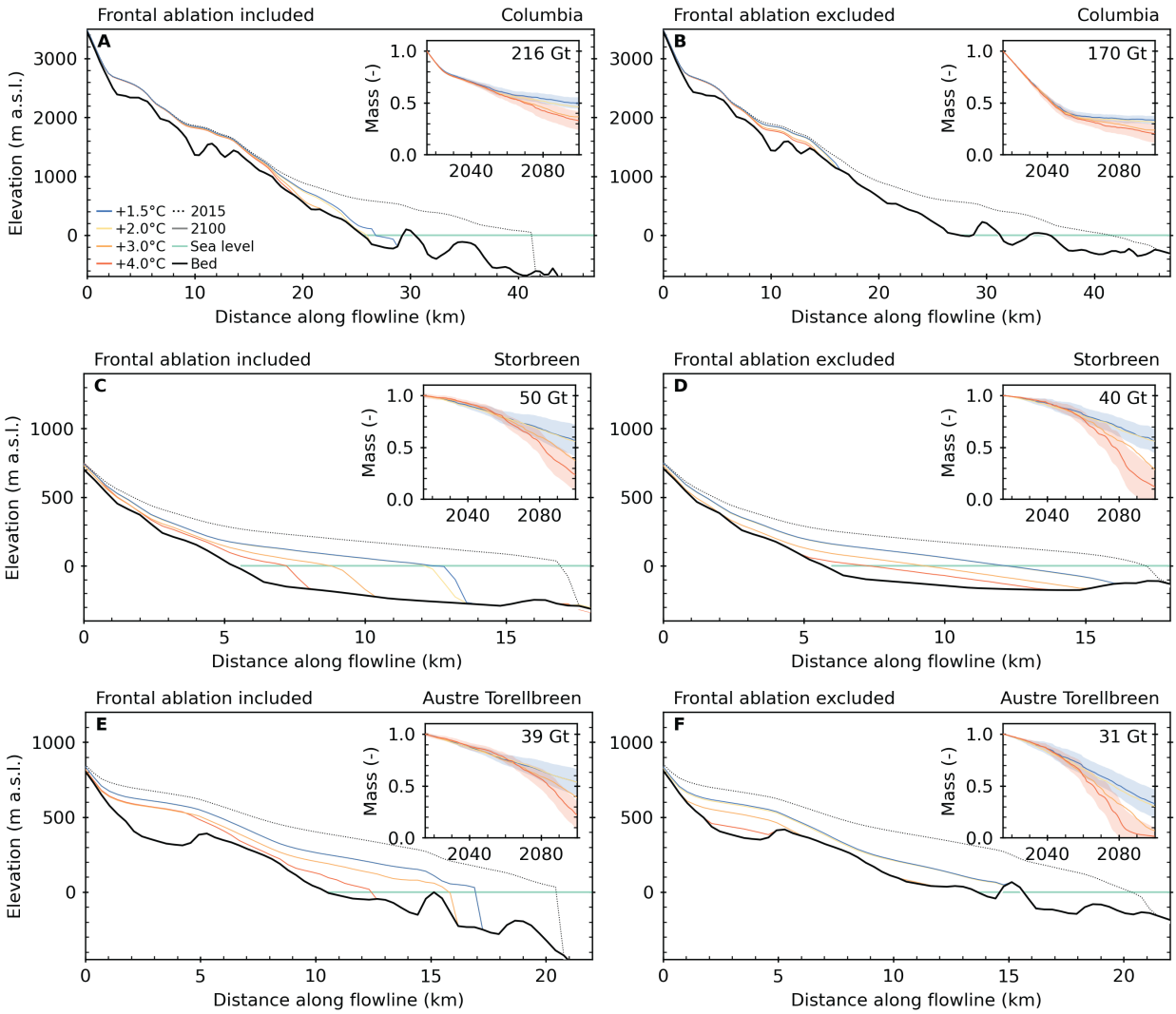

Fig. S14.
Impact of frontal ablation on projected mass change for Columbia Glacier, Alaska; Storbreen, Svalbard; and Austre Torellbreen, Svalbard. Surface elevation along the glacier flowline at 2100 for ensembles of temperature change scenarios (colored lines) with frontal ablation (A, C, E) included and (B, D, F) excluded in the simulations. Insets show mass change relative to 2015. Text shows the mass in Gt in 2015. The bed topography is internally derived for each model run so the ice thickness is consistent with the mass-balance gradient, and therefore differs between the two cases.

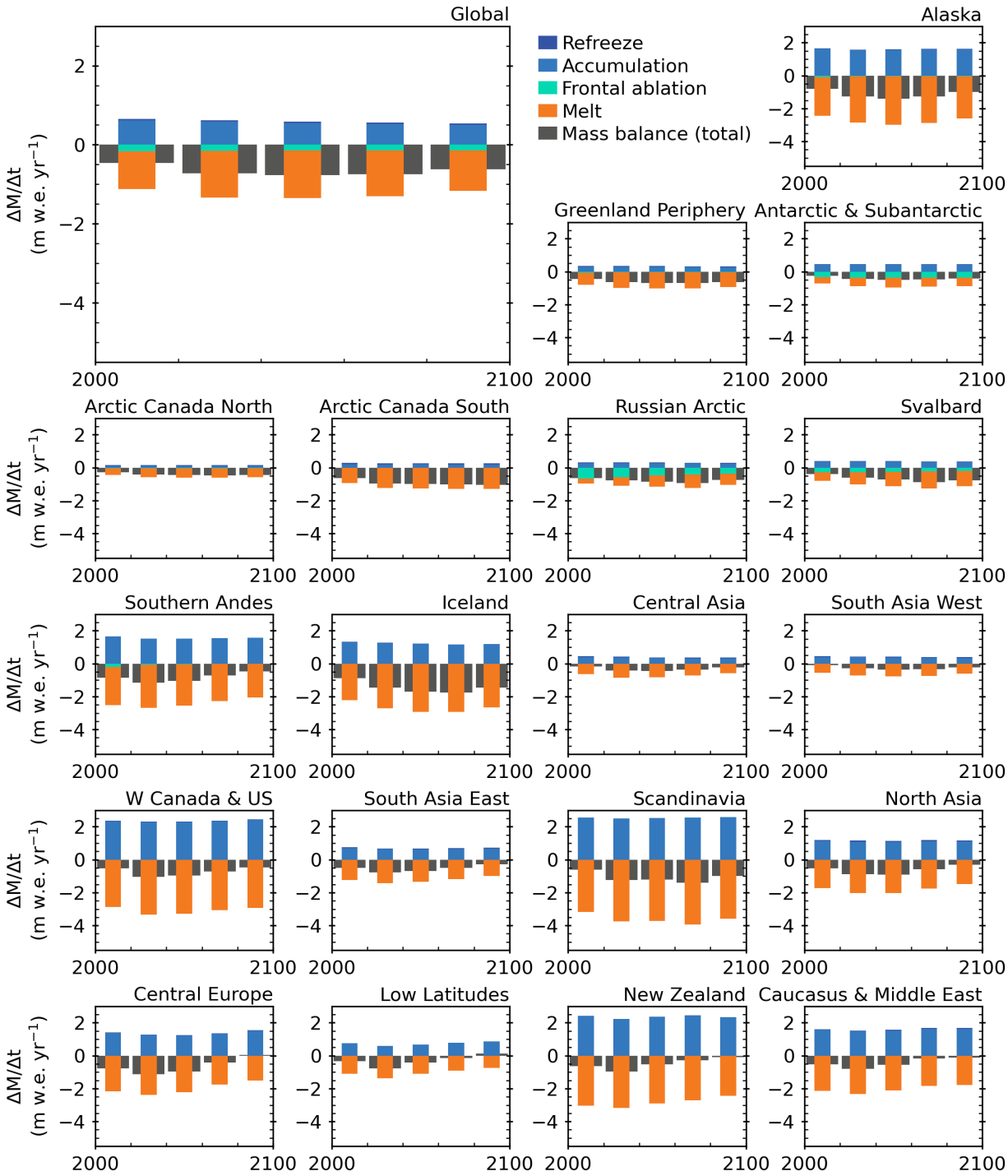

Fig. S15.
Global and regional mass balance components from 2000 to 2100 for the +1.5°C global mean temperature scenario by 2100 relative to pre-industrial levels. Components are averaged over 20-year periods. Regions are ordered by their total mass loss.

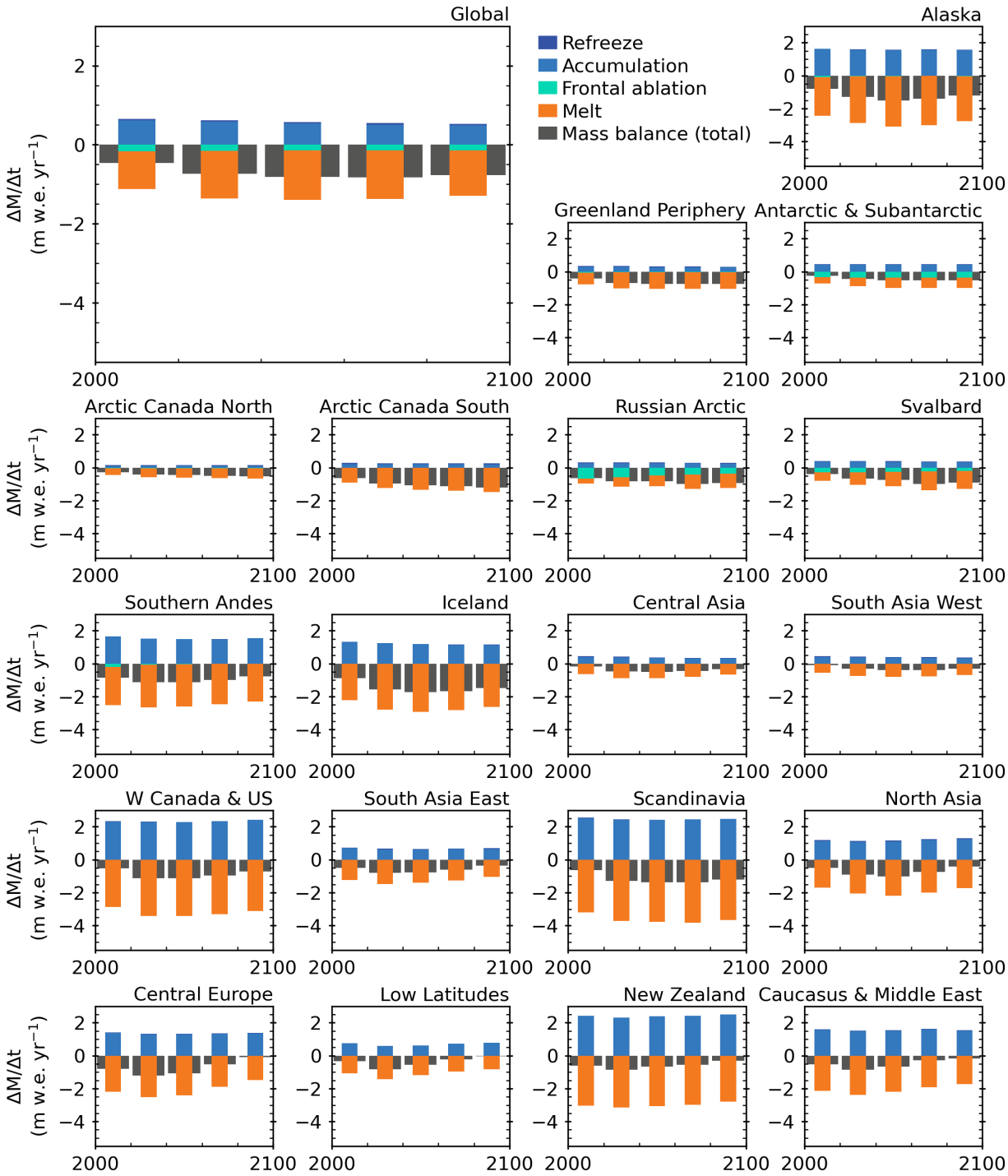

Fig. S16.
Global and regional mass balance components from 2000 to 2100 for the +2°C global mean temperature scenario by 2100 relative to pre-industrial levels. Components are averaged over 20-year periods. Regions are ordered by their total mass loss.

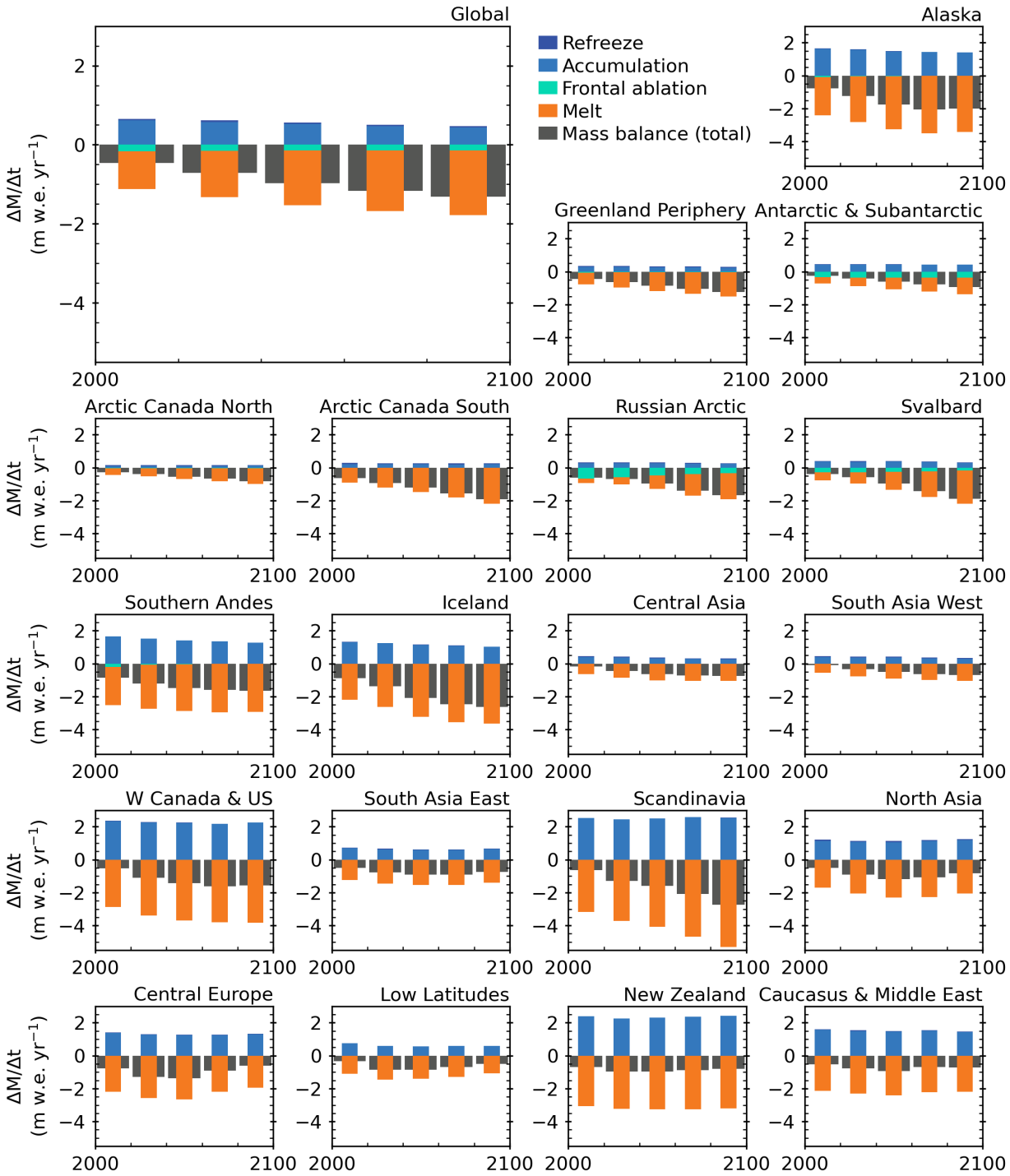

Fig. S17.
Global and regional mass balance components from 2000 to 2100 for the +3°C global mean temperature scenario by 2100 relative to pre-industrial levels. Components are averaged over 20-year periods. Regions are ordered by their total mass loss.

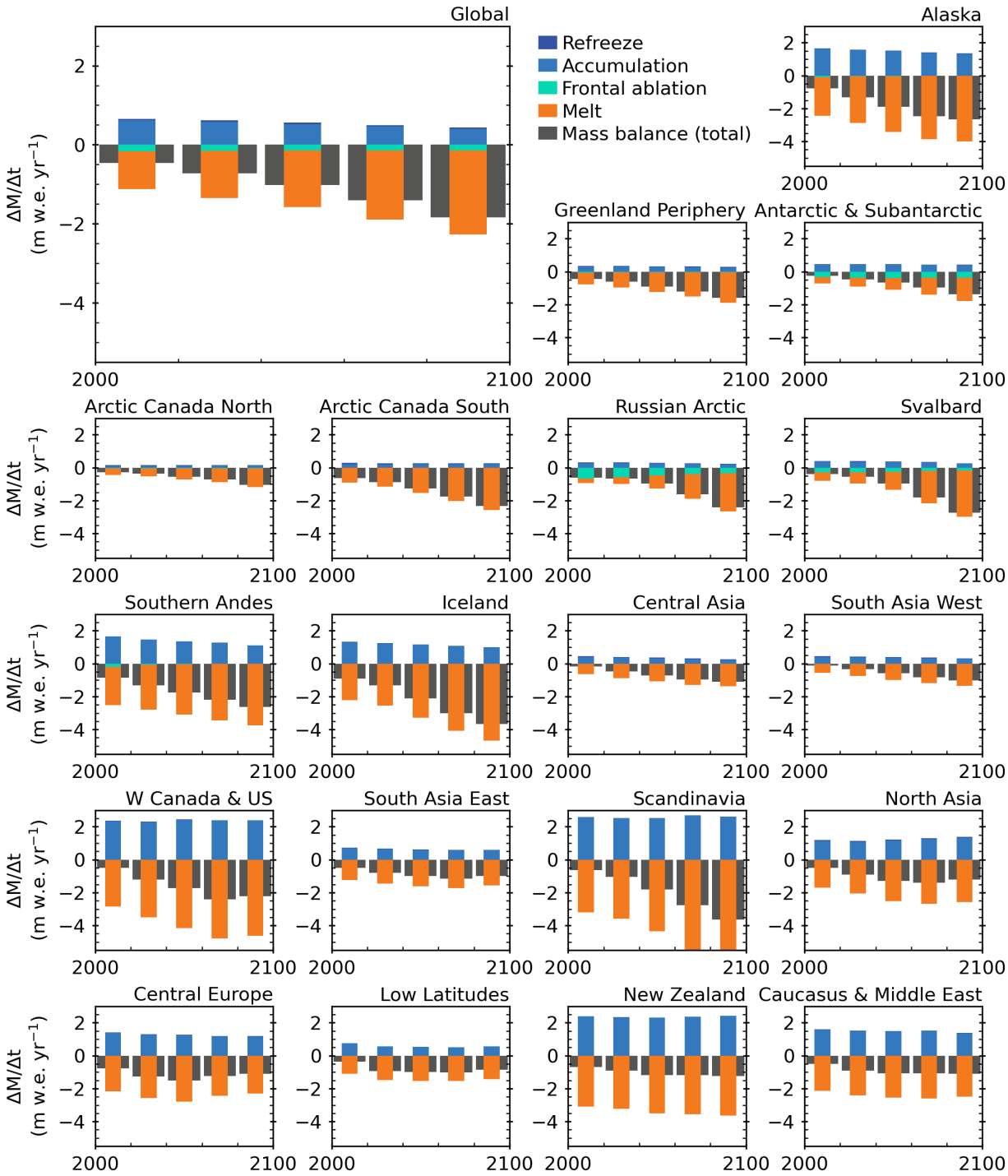

Fig. S18.
Global and regional mass balance components from 2000 to 2100 for the +4°C global mean temperature scenario by 2100 relative to pre-industrial levels. Components are averaged over 20-year periods. Regions are ordered by their total mass loss.

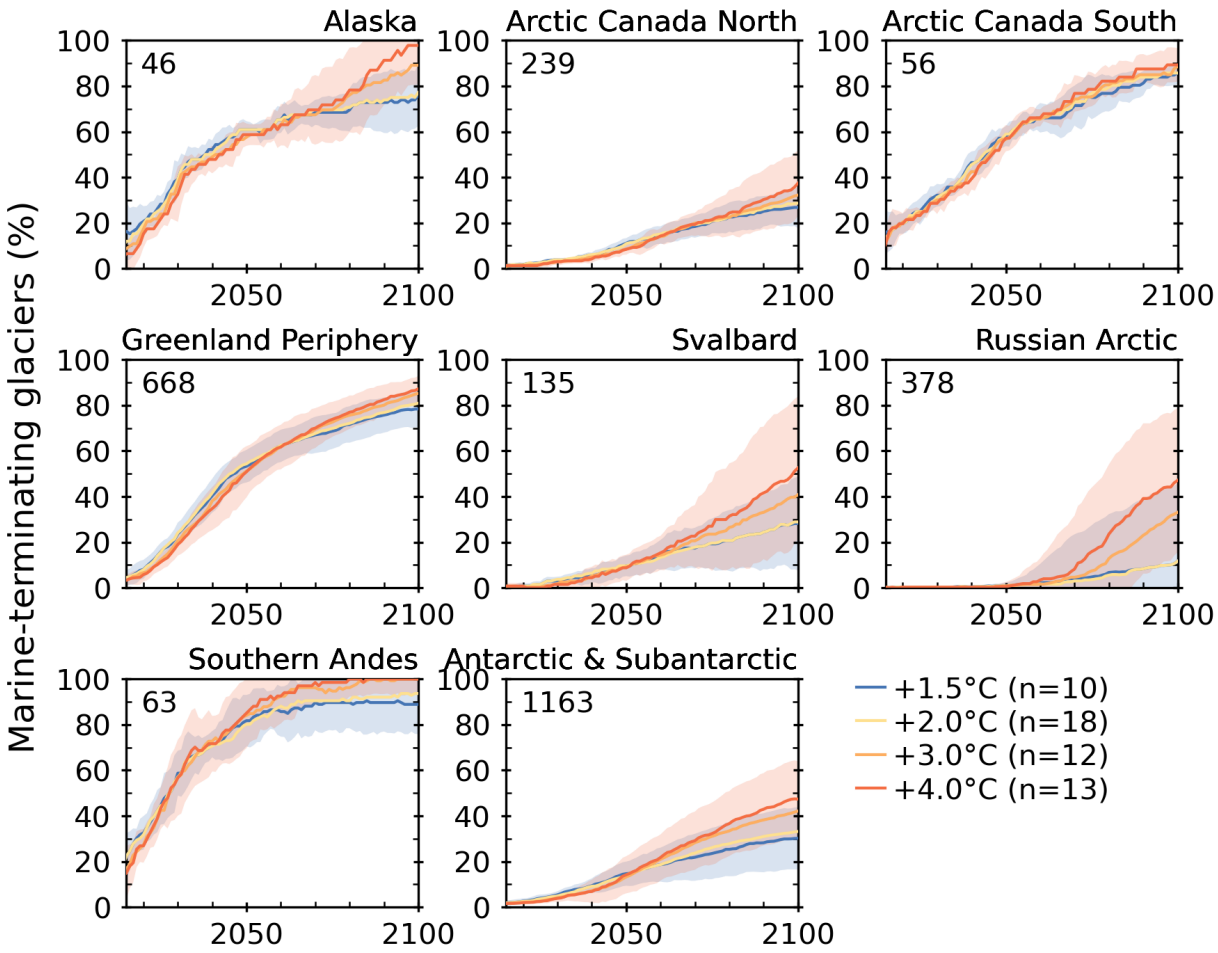

Fig. S19.
Regional percentage of marine-terminating glaciers that retreat to land from 2015 to 2100 for various temperature change scenarios. Four global mean temperature change scenarios are based on 2100 relative to pre-industrial levels. Text denotes the number of marine-terminating glaciers simulated in each region.

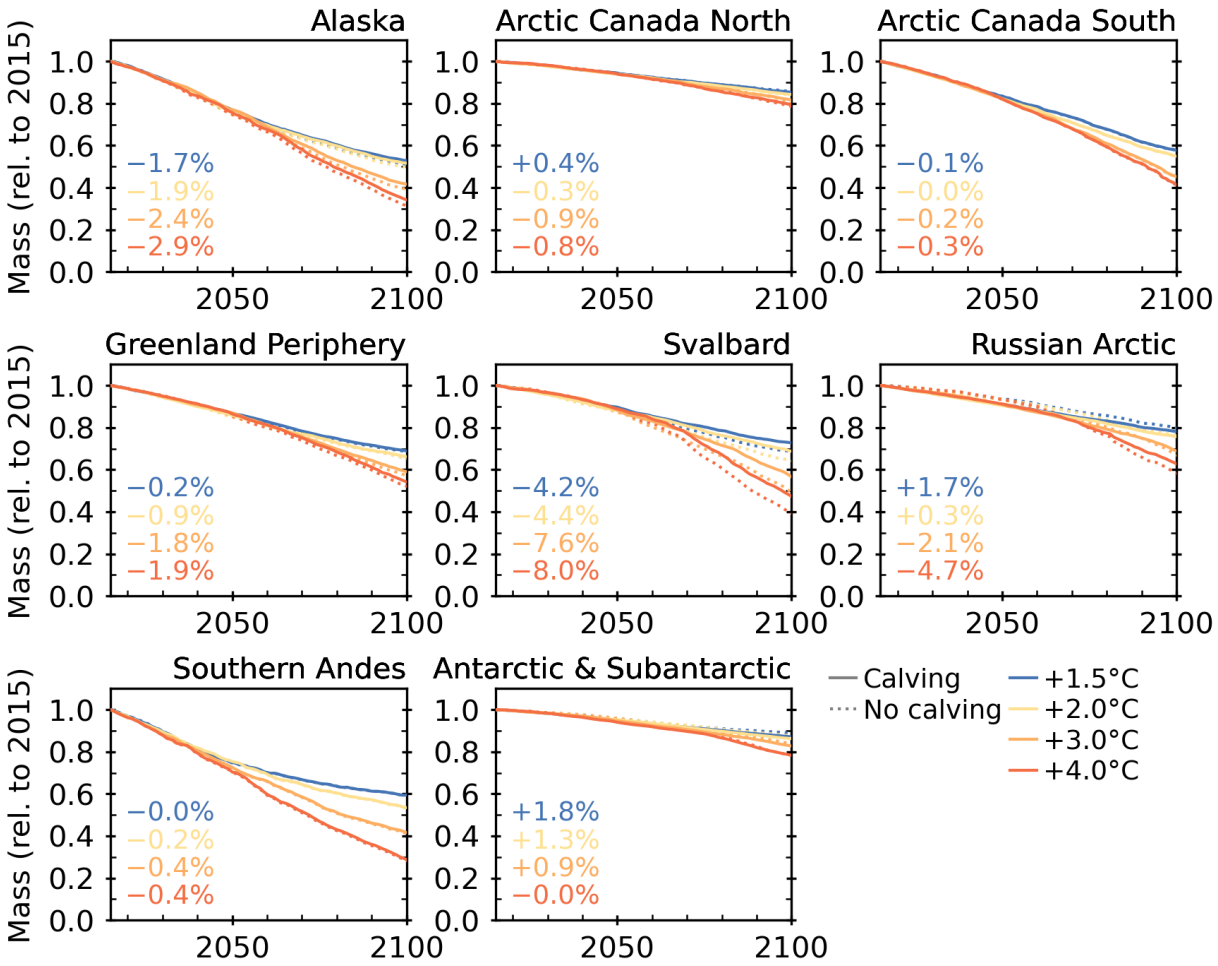

Fig. S20.
Impact of frontal ablation on projected mass change. Regional glacier mass evolution, relative to 2015, for four global mean temperature change scenarios by 2100 relative to pre-industrial levels (colors) accounting for frontal ablation (solid lines) and treating marine-terminating glaciers as land-terminating glaciers (dotted lines) for various regions with marine-terminating glaciers. Text shows the percent change of not accounting for frontal ablation compared to when it is included.

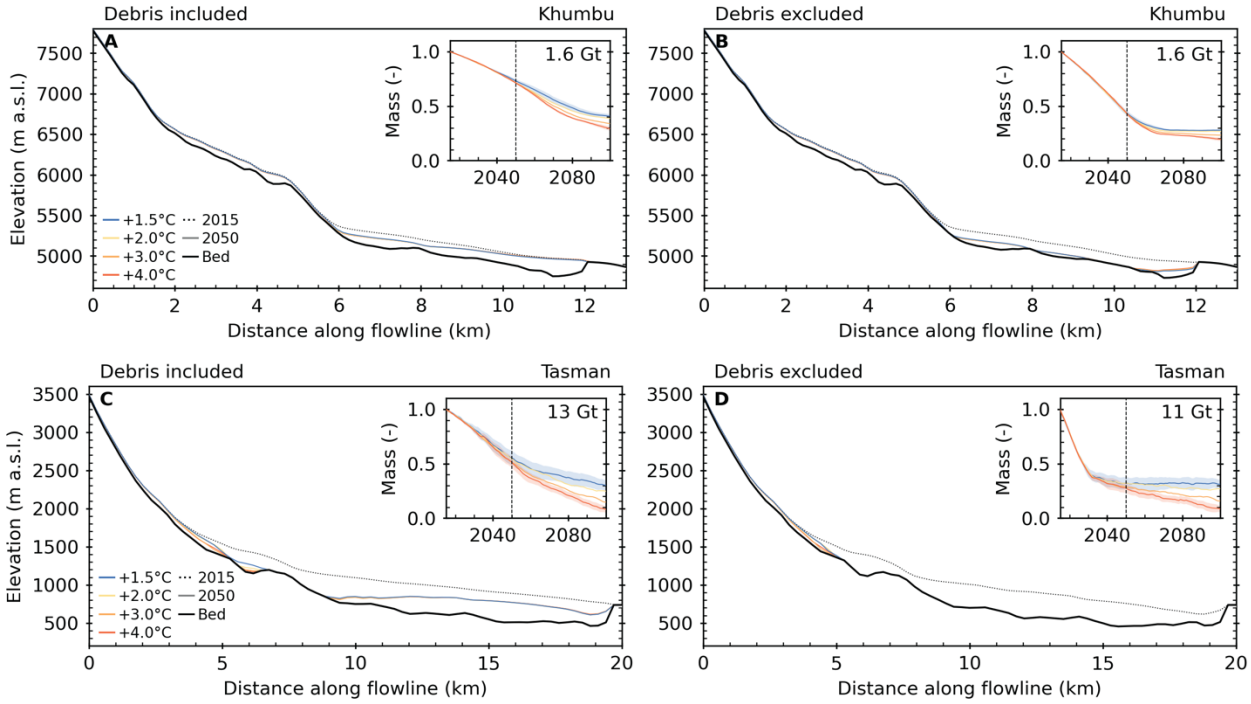

Fig. S21.
Impact of accounting for debris cover on projected mass change for Khumbu Glacier, Nepal and Tasman Glacier, New Zealand. Surface elevation along the glacier flowline at 2050 for ensembles of temperature change scenarios (colored lines) with debris (A, C) included and (B, D) excluded in the simulations. The cross sections are shown in 2050 to showcase the inverted mass balance gradient and separation of glacier tongues. Insets show mass change relative to 2015. Text shows the mass in Gt in 2015. The bed topography is internally derived for each model run so the ice thickness is consistent with the mass-balance gradient, and therefore the bed topography and initial mass differs between the two cases.

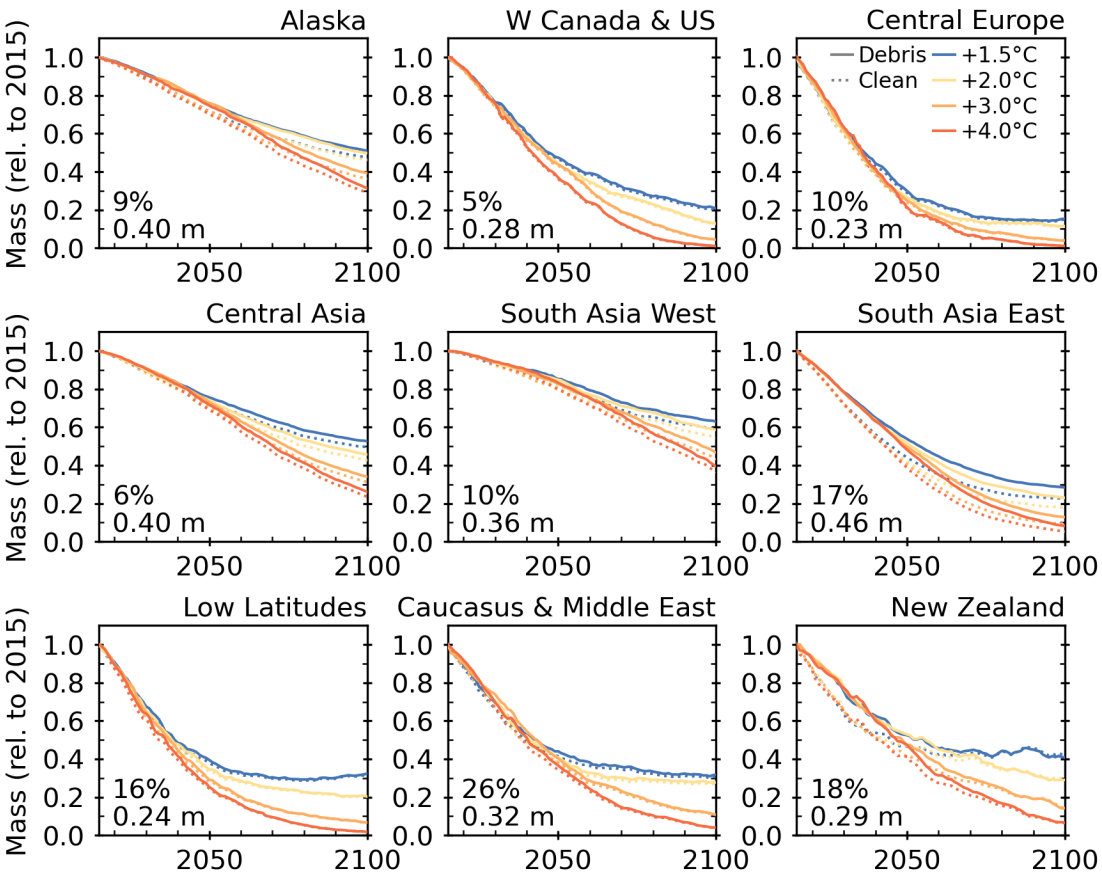

Fig. S22.
Impact of debris cover on projected mass change. Regional glacier mass evolution, relative to 2015, for four global mean temperature change scenarios by 2100 relative to pre-industrial levels accounting for debris compared to assuming clean ice in place of debris for various regions with significant debris-covered areas. Text shows the percent debris cover by area (*24*) and mean debris thickness (*17*).

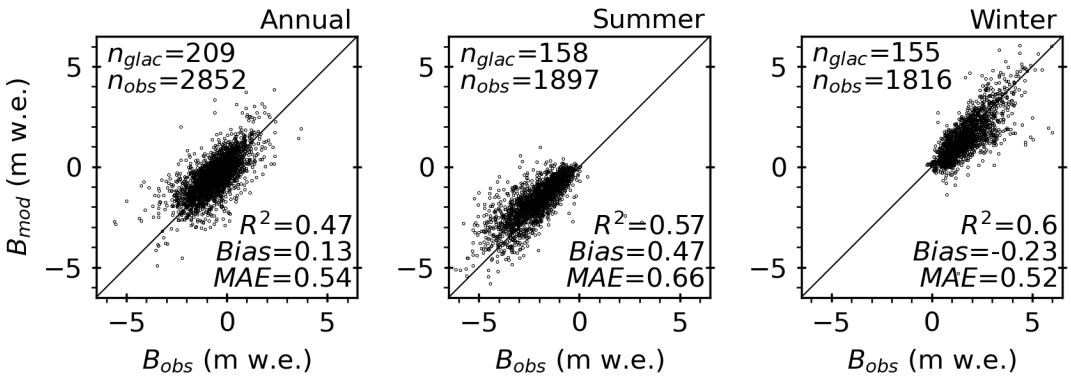

Fig. S23.
Validation of modeled glacier-wide mass balance (B_{mod}) compared to glaciological observations (B_{obs}) at annual and seasonal timescales (*32*). Validation for each region at annual and seasonal timescales are shown in Figs. S24-26. Bias and mean absolute error (MAE) shown in m w.e.

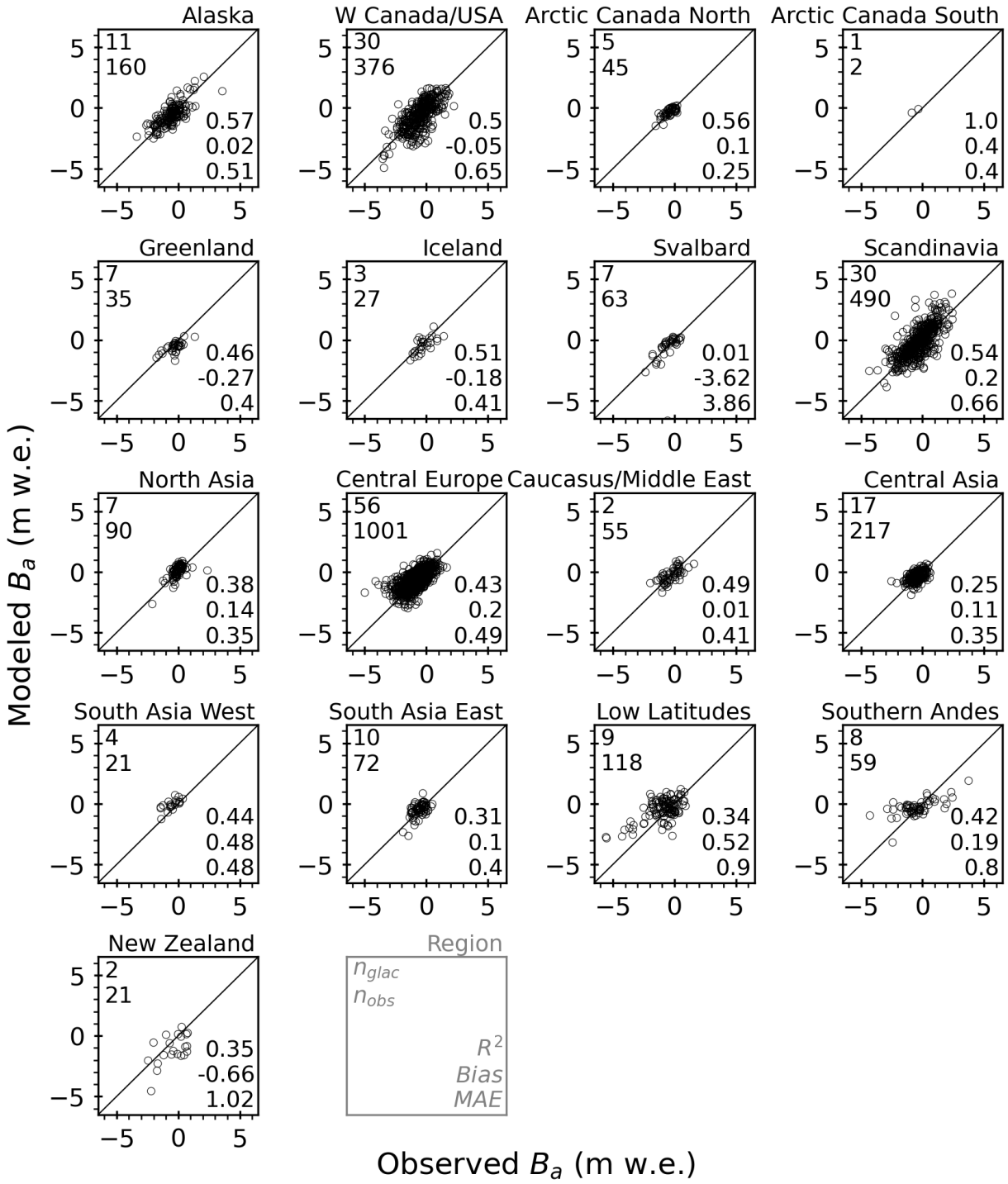

Fig. S24.
Validation of modeled annual glacier-wide mass balance (B_a) compared to glaciological observations for each region with data (*32*). The legend is in grey showing the number of glaciers (n_{glac}) and observations (n_{obs}) in upper left and correlation of determination (R^2), bias (m w.e. yr^{-1}), and mean absolute error (*MAE*; m w.e. yr^{-1}) in lower right.

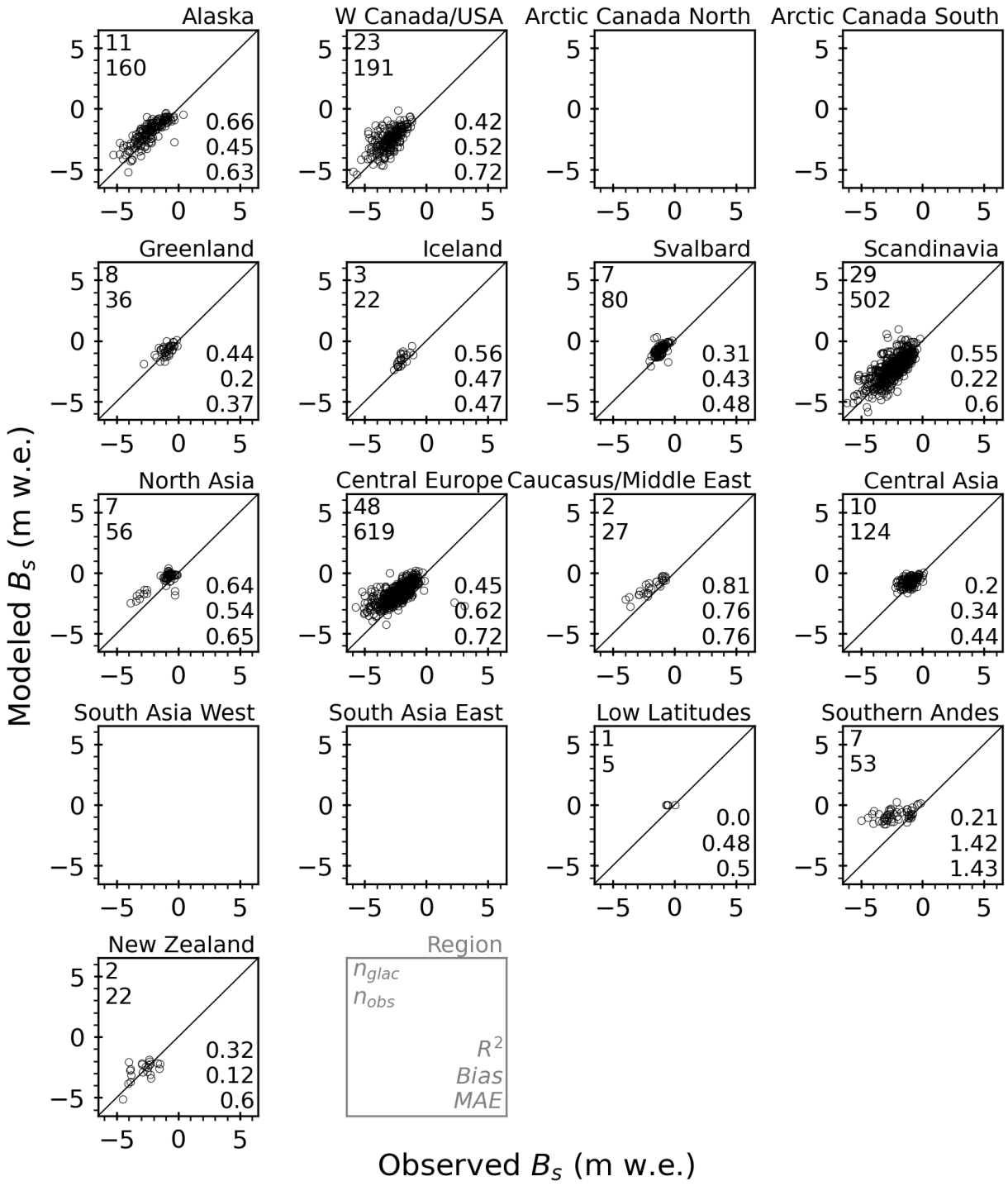

Fig. S25.
Validation of modeled summer glacier-wide mass balance (B_s) compared to glaciological observations for each region with data (*32*). Empty plots indicate regions with annual data, but no summer data. The legend is in grey showing the number of glaciers (n_{glac}) and observations (n_{obs}) in upper left and correlation of determination (R^2), bias (m w.e.), and mean absolute error (*MAE*; m w.e.) in lower right.

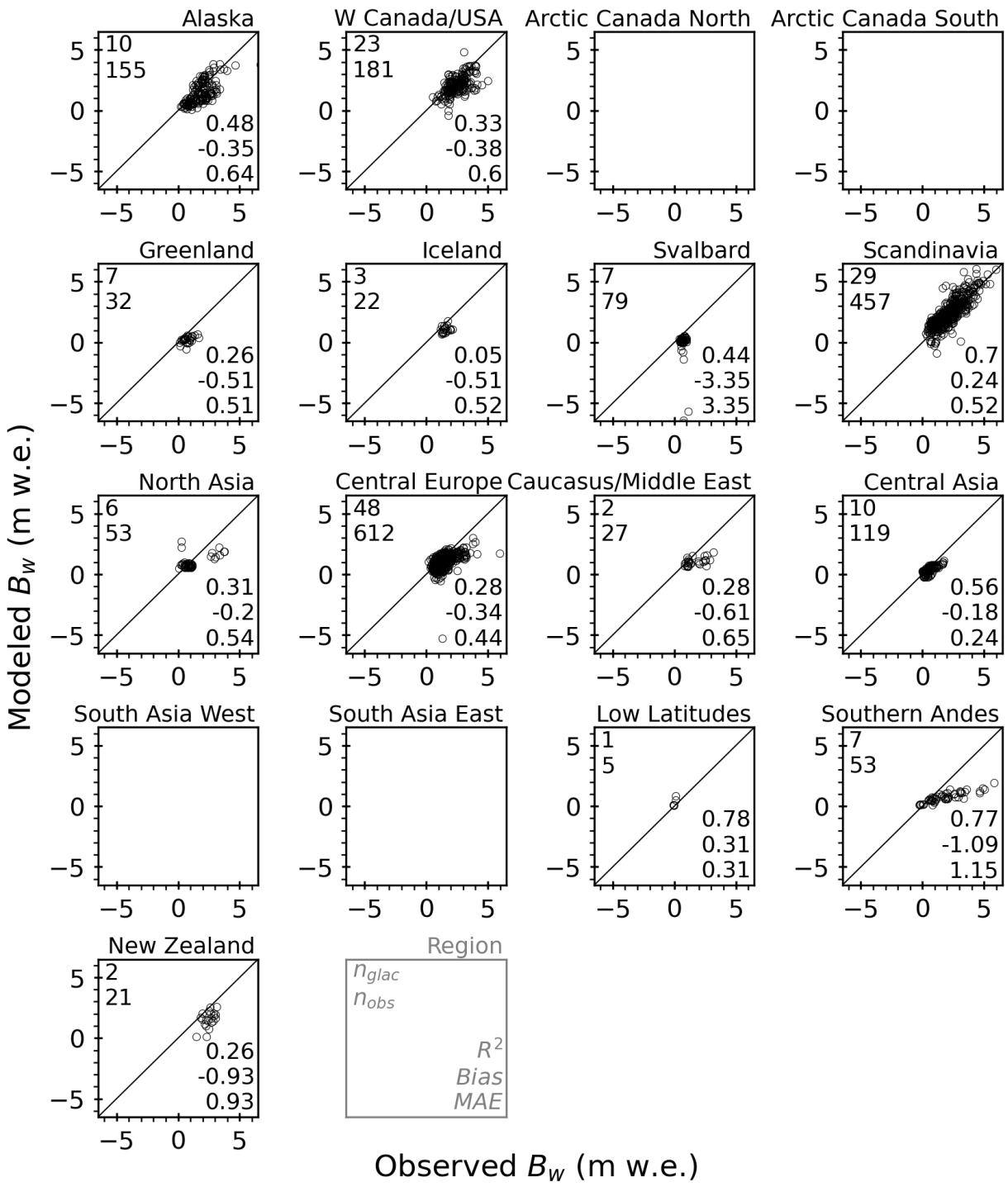

Fig. S26.
Validation of modeled winter glacier-wide mass balance (B_w) compared to glaciological observations for each region with data (*32*). Empty plots indicate regions with annual data, but no winter data. The legend is in grey showing the number of glaciers (n_{glac}) and observations (n_{obs}) in upper left and correlation of determination (R^2), bias (m w.e.), and mean absolute error (*MAE*; m w.e. yr^{-1}) in lower right.

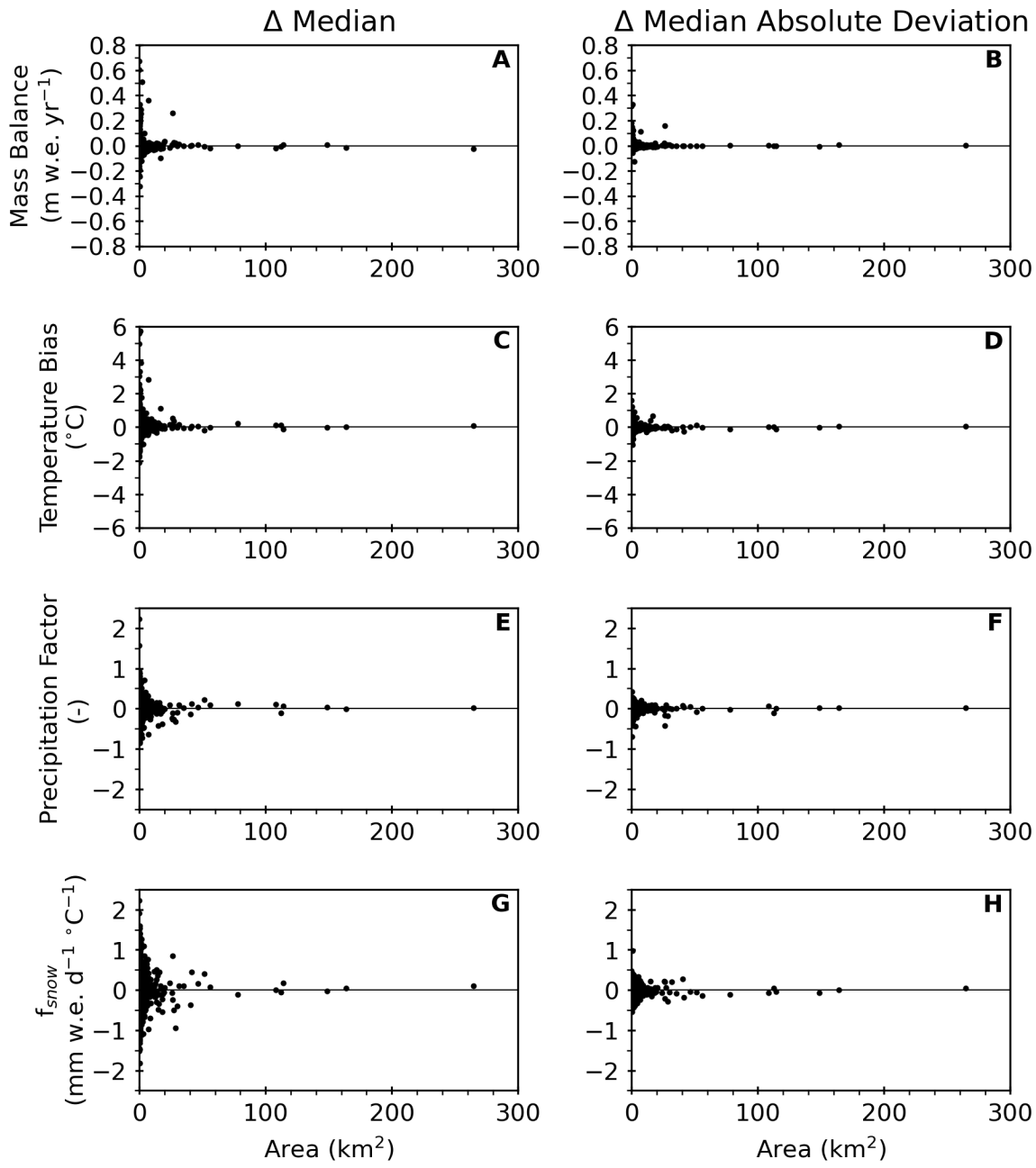

Fig. S27.
Comparison of posterior distributions as a function of glacier area when applying the Markov Monte Chain Methods using the emulator versus the full model. Differences in the median and median absolute deviation versus initial glacier area for the (A, B) posterior predictive distribution for the mass balance and marginal posterior distributions for the (C, D) temperature bias, (E, F) precipitation factor, and (G, H) degree-day factor of snow (f_{snow}) for 2500 randomly selected glaciers.

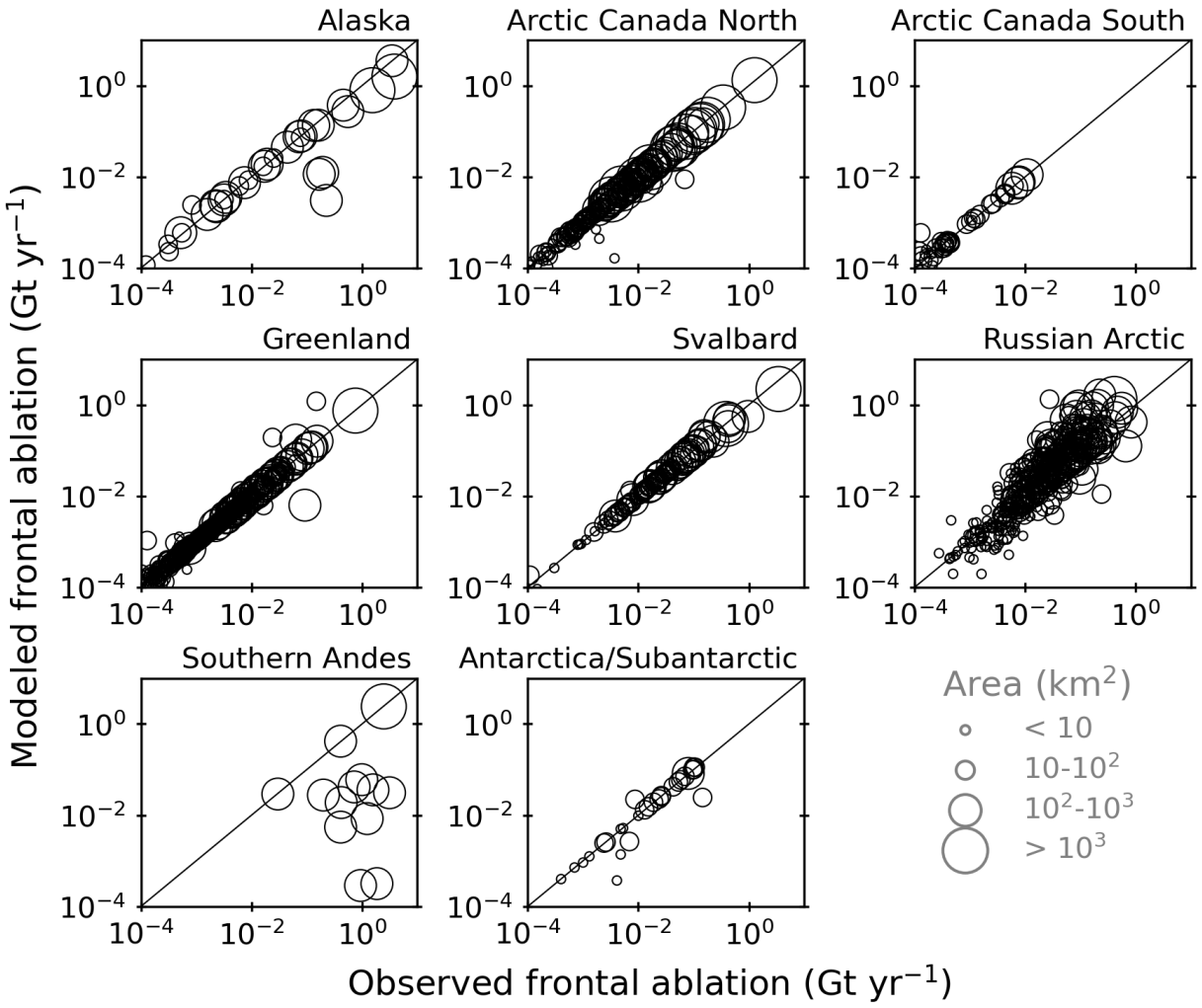

Fig. S28.
Comparison of modeled and observed frontal ablation rates of marine-terminating glaciers after calibration for each region with marine-terminating glaciers. Area refers to the area of each marine-terminating glacier.

Table S1.

Percentage of projected global and regional glacier mass loss by 2100, relative to 2015, for RCP scenarios from this study and a recent multi-model study (*2*). In 47 of the 57 regional cases, the regional relative mass losses (ensemble medians) are greater than the multi-model study (those greater than 15% are bolded). Note that uncertainty associated with Marzeion et al. (*2*) is expressed as 90% confidence interval based on up to 11 glacier models and 10 GCMs. This study reports ensemble median and 95% confidence interval. Projections for SSPs are shown in Table S5.

	RCP2.6		RCP4.5		RCP8.5	
Region	This study	Marzeion et al. (*2*)	This study	Marzeion et al. (*2*)	This study	Marzeion et al. (*2*)
Alaska	**49±16**	27±21	**54±16**	32±24	**67±18**	44±27
W Canada & US	76±21	64±30	**94±19**	78±29	99±6	90±23
Arctic Canada North	16±8	12±13	18±8	18±13	24±13	27±18
Arctic Canada South	**41±26**	23±27	46±26	33±30	**63±24**	48±32
Greenland Periphery	34±15	22±24	37±15	29±26	55±18	42±29
Iceland	38±27	30±35	50±34	40±47	62±37	55±45
Svalbard	27±12	35±34	39±29	50±36	57±33	66±36
Scandinavia	**72±33**	53±34	**87±22**	68±34	93±9	84±24
Russian Arctic	21±11	26±26	27±23	38±29	43±26	52±31
North Asia	**77±22**	62±41	87±10	79±38	95±5	90±30
Central Europe	78±14	68±31	93±9	83±22	99±3	95±13
Caucasus & Middle East	71±27	68±33	79±14	83±19	97±4	94±13
Central Asia	45±26	44±28	63±23	61±24	80±17	74±19
South Asia West	34±19	34±26	53±23	48±28	69±20	63±27
South Asia East	**71±15**	50±38	**83±10**	67±35	94±4	83±27
Low Latitudes	69±25	74±43	88±11	89±24	98±2	98±13
Southern Andes	**38±15**	23±27	**49±17**	30±27	**68±20**	46±26
New Zealand	53±25	44±45	**74±18**	58±33	93±9	79±27
Antarctic & Subantarctic	11±5	7±12	15±7	13±11	20±14	16±19
Global	26±8	18±13	31±10	27±15	43±13	36±20

Table S2.

Projected global and regional glacier contribution to sea-level rise (mm SLE) by 2100, relative to 2015, for RCP scenarios from this study and a recent multi-model study (*2*). Global excluding Greenland Periphery (G) and Antarctic and Subantarctic (A) are shown as well. 'Uncorrected' refers to the projections that assume mass losses below sea level contribute to sea-level rise, consistent with assumptions in the multi-model studies. Note that uncertainty associated with Marzeion et al. (*2*) is expressed as 90% confidence interval based on up to 11 glacier models and 10 GCMs. This study reports ensemble median and 95% confidence interval. Projections for SSPs are shown in Table S5.

	RCP2.6			RCP4.5			RCP8.5		
Region	This study	This study (uncorrected)	Marzeion et al. (*2*)	This study	This study (uncorrected)	Marzeion et al. (*2*)	This study	This study (uncorrected)	Marzeion et al. (*2*)
Alaska	22±8	22±8	14±11	24±8	25±8	19±13	31±9	31±9	25±15
W Canada & US	2±1	2±1	1±1	2±0	2±0	2±1	2±0	2±0	2±1
Arctic Canada North	11±6	12±7	10±10	12±6	13±6	16±15	17±10	19±11	24±20
Arctic Canada South	8±6	8±6	5±6	10±6	10±6	7±7	13±6	13±6	11±7
Greenland Periphery	12±6	13±6	9±10	13±6	14±6	12±11	21±7	22±8	18±11
Iceland	4±3	4±3	2±3	5±4	5±4	4±4	6±4	6±4	5±3
Svalbard	5±2	6±3	7±7	7±6	8±7	11±9	11±7	12±8	14±8
Scandinavia	0±0	0±0	0±0	1±0	1±0	0±0	1±0	1±0	0±0
Russian Arctic	5±4	9±5	10±8	8±9	12±11	14±11	14±10	19±13	20±12
North Asia	0±0	0±0	0±0	0±0	0±0	0±0	0±0	0±0	0±0
Central Europe	0±0	0±0	0±0	0±0	0±0	0±0	0±0	0±0	0±0
Caucasus & Middle East	0±0	0±0	0±0	0±0	0±0	0±0	0±0	0±0	0±0
Central Asia	4±2	4±2	4±3	5±2	5±2	6±3	7±2	7±2	6±4
South Asia West	2±1	2±1	3±2	4±2	4±2	4±2	5±2	5±2	5±3
South Asia East	1±0	1±0	1±1	2±0	2±0	2±1	2±0	2±0	2±1
Low Latitudes	0±0	0±0	0±0	0±0	0±0	0±0	0±0	0±0	0±0
Southern Andes	5±2	5±2	3±4	6±2	6±2	4±3	9±3	9±3	6±4
New Zealand	0±0	0±0	0±0	0±0	0±0	0±0	0±0	0±0	0±0
Antarctic & Subantarctic	6±5	15±7	9±15	10±7	20±10	16±13	15±14	27±21	20±24
Global (excl. A & G)	70±30	77±31	61±41	89±37	95±40	91±53	124±41	133±46	121±64
Global	90±36	106±37	79±56	114±44	132±47	119±66	163±53	187±61	159±86

Table S3.

Ensemble of GCMs, RCPs, and SSPs used to force the glacier evolution model from 2000-2100. In total, 82 climate projections were used.

Scenario	Number of GCMs	GCMs
SSP1-1.9	4	EC-Earth3, EC-Earth3-Veg, GFDL-ESM4, MRI-ESM2-0
SSP1-2.6 SSP2-4.5 SSP3-7.0 SSP5-8.5	12	BCC-CSM2-MR, CESM2, CESM2-WACCM, EC-Earth3, EC-Earth3-Veg, FGOALS-f3-L, GFDL-ESM4, INM-CM4-8, INM-CM5-0, MPI-ESM1-2-HR, MRI-ESM2-0, NorESM2-MM
RCP2.6 RCP4.5 RCP8.5	10	CanESM2, CCSM4, CNRM-CM5, CSIRO-Mk3-6-0, GFDL-CM3, GFDL-ESM2M, GISS-E2-R, IPSL-CM5A-LR, MPI-ESM-LR, NorESM1-M

Table S4.
Global and regional ice volume in 2015 reporting ensemble median and 95% confidence interval.

Region	+1.5°C	+2°C	+3°C	+4°C
Alaska	18.45±0.45	18.62±0.50	18.75±0.28	18.92±0.39
W Canada & US	0.95±0.05	0.96±0.07	0.97±0.04	0.97±0.05
Arctic Canada North	29.15±1.09	29.40±1.33	29.89±1.66	30.39±1.54
Arctic Canada South	8.42±0.20	8.47±0.15	8.53±0.17	8.57±0.17
Greenland Periphery	15.42±0.37	15.55±0.43	15.76±0.44	15.90±0.33
Iceland	3.88±0.11	3.87±0.14	3.94±0.17	3.98±0.16
Svalbard	8.36±0.35	8.41±0.29	8.61±0.32	8.81±0.39
Scandinavia	0.28±0.01	0.28±0.01	0.28±0.01	0.28±0.01
Russian Arctic	17.58±0.57	17.72±0.50	17.91±0.55	18.17±0.55
North Asia	0.11±0.00	0.11±0.01	0.12±0.00	0.12±0.00
Central Europe	0.11±0.01	0.11±0.01	0.11±0.01	0.11±0.01
Caucasus & Middle East	0.05±0.00	0.05±0.00	0.05±0.00	0.05±0.00
Central Asia	3.20±0.06	3.25±0.09	3.32±0.06	3.39±0.05
South Asia West	2.76±0.05	2.79±0.09	2.86±0.08	2.92±0.07
South Asia East	0.77±0.01	0.78±0.02	0.79±0.02	0.80±0.01
Low Latitudes	0.09±0.00	0.09±0.01	0.09±0.00	0.09±0.00
Southern Andes	5.06±0.09	5.09±0.11	5.18±0.10	5.22±0.12
New Zealand	0.06±0.00	0.06±0.01	0.06±0.01	0.07±0.01
Antarctic & Subantarctic	54.10±1.39	54.36±1.49	55.50±1.78	56.59±1.79
Global	168.87±2.91	170.35±3.66	172.93±4.01	175.15±3.93

Table S5.

Percentage of projected global and regional glacier mass loss by 2100, relative to 2015, and glacier contribution to sea-level rise (mm SLE) from 2015 to 2100 for SSP scenarios. Global excluding Greenland Periphery (G) and Antarctic and Subantarctic (A) are shown as well. The reported values are the ensemble median and 95% confidence interval.

	Mass loss, relative to 2015 (%)				Sea level rise contribution, 2015-2100 (mm SLE)			
Region	SSP1-2.6	SSP2-4.5	SSP3-7.0	SSP5-8.5	SSP1-2.6	SSP2-4.5	SSP3-7.0	SSP5-8.5
Alaska	51±17	58±20	66±20	73±24	23±8	27±10	31±10	34±12
W Canada & US	87±13	95±8	99±5	99±3	2±0	2±0	2±0	2±0
Arctic Canada North	15±11	18±15	21±21	24±30	10±9	12±12	15±17	17±23
Arctic Canada South	45±15	53±17	60±21	66±27	9±3	11±4	13±5	14±6
Greenland Periphery	33±14	39±16	45±22	50±27	12±6	14±7	17±9	19±11
Iceland	39±23	48±26	55±26	62±27	4±2	5±3	5±3	6±3
Svalbard	29±22	37±28	49±31	64±29	5±4	7±6	9±7	12±6
Scandinavia	75±19	88±17	94±9	96±7	1±0	1±0	1±0	1±0
Russian Arctic	23±14	27±20	36±24	43±26	6±5	8±8	11±9	14±10
North Asia	81±10	89±6	93±5	95±4	0±0	0±0	0±0	0±0
Central Europe	86±8	95±4	99±2	100±1	0±0	0±0	0±0	0±0
Caucasus & Middle East	71±9	87±6	95±3	98±2	0±0	0±0	0±0	0±0
Central Asia	50±10	62±7	72±7	81±9	4±1	5±1	6±1	7±1
South Asia West	41±16	49±16	58±17	68±19	3±1	3±1	4±1	5±2
South Asia East	77±12	86±8	92±5	94±5	1±0	2±0	2±0	2±0
Low Latitudes	76±18	91±9	97±4	99±3	0±0	0±0	0±0	0±0
Southern Andes	49±19	57±19	68±21	74±22	6±3	7±3	9±3	9±3
New Zealand	64±21	80±13	93±8	95±7	0±0	0±0	0±0	0±0
Antarctic & Subantarctic	14±6	16±8	22±10	26±15	9±7	11±8	17±10	21±14
Global	28±9	32±12	39±15	44±20	98±38	116±51	147±64	166±83